bioRxiv preprint doi: https://doi.org/10.1101/719864; this version posted August 8, 2019. The copyright holder for this preprint (which was not certified by peer review) is the author/funder, who has granted bioRxiv a license to display the preprint in perpetuity. It is made available under aCC-BY-NC-ND 4.0 International license.

Aging-associated changes in transcriptional elongation influence metazoan longevity

Cédric Debès[1#], Sebastian Grönke[2#], Özlem Karalay[2#], Luke Tain[2], Shuhei Nakamura[2], Oliver Hahn[1,2], Carina Weigelt[2], Anne Zirkel[5], Konstantinos Sofiadis[5], Lilija Brant[5], Bernd Wollnik[7], Torsten Kubacki[3], Martin Späth[3], Bernhard Schermer[1,3,4,5], Thomas Benzing[1,3,4,5], Roman-Ulrich Müller[1,3,4], Argyris Papantonis[8*], Adam Antebi[2,4*], Linda Partridge[2,4,6*], Andreas Beyer[1,4,5*]

Affiliations:

[1]CECAD, University of Cologne, Faculty of Medicine and University Hospital Cologne, Cologne, Germany.

[2]Max Planck Institute for Biology of Aging, Joseph-Stelzmann-Str. 9b, 50931 Cologne, Germany.

[3]Department II of Internal Medicine and Center for Molecular Medicine Cologne, University of Cologne, Faculty of Medicine and University Hospital Cologne, Cologne, Germany.

[4]Systems Biology of Aging Cologne, University of Cologne, 50923 Cologne, Germany.

[5]Center for Molecular Medicine of the University of Cologne, 50931 Cologne, Germany.

[6]Institute of Healthy Aging, Department of Genetics, Evolution and Environment, UCL, London WC1E 6BT, UK.

[7]University Medical Center Göttingen, 37073 Göttingen, Germany.

[8]Institute of Pathology, University Medical Centre Göttingen, 37075 Göttingen, Germany.

# These authors contributed equally to this work.

*Correspondence to: Email: argyris.papantonis@med.uni-goettingen.de (A.P.); aantebi@age.mpg.de (A.A.); Partridge@age.mpg.de (L.P.); andreas.beyer@uni-koeln.de (A.B.)

bioRxiv preprint doi: https://doi.org/10.1101/719864; this version posted August 8, 2019. The copyright holder for this preprint (which was not certified by peer review) is the author/funder, who has granted bioRxiv a license to display the preprint in perpetuity. It is made available under aCC-BY-NC-ND 4.0 International license.

Abstract

Aging impairs cellular homeostasis, thereby compromising multiple cellular processes, including transcription and splicing. However, the molecular mechanisms at work, and hence ways of preventing loss of transcriptional fidelity, are so far elusive. We analyzed changes in genome-wide, transcription-coupled processes with age in *Caenorhabditis elegans, Drosophila melanogaster, Mus musculus, Rattus norvegicu*s and *Homo sapiens*. Using total RNA profiling, we quantified transcriptional elongation speed (Pol-II speed). Genome-averaged Pol-II speed increased with age in all five species. Lifespan-extending dietary restriction and lowered insulin signaling both rescued these age-related trends. Experimentally reducing Pol-II speed in worms and flies increased lifespan. These findings uncover fundamental molecular mechanisms driving animal aging and underlying lifespan-extending interventions, and point to possible preventative measures.

One-sentence summary

Genome-wide analysis of total RNA during aging reveals increased transcriptional elongation speed and decreased splicing efficiency, with an impact on longevity.

bioRxiv preprint doi: https://doi.org/10.1101/719864; this version posted August 8, 2019. The copyright holder for this preprint (which was not certified by peer review) is the author/funder, who has granted bioRxiv a license to display the preprint in perpetuity. It is made available under aCC-BY-NC-ND 4.0 International license.

Main Text

Aging impairs a wide range of cellular processes, many of which affect the quality and concentration of proteins. Among these, transcription is particularly important, because it is the main regulator of protein levels (*1-3*). Transcriptional elongation is critical for proper mRNA synthesis, due to its association with pre-mRNA processing steps such as splicing, editing, and 3' end formation (*4*, *5*). Indeed, dysregulation of transcriptional elongation can lead to a number of diseases (*6*). During aging, animal transcriptomes undergo extensive remodeling, with large-scale changes in expression of transcripts involved in signaling pathways, DNA damage response, protein homeostasis (e.g. the ubiquitin-proteasome pathway), immune response, and stem cell plasticity (*7*). Further, some studies detected an age-related increase in variability and error of gene expression (*8-10*). This prior work has provided insights into how the transcriptome adapts to, and is affected by, aging-associated cellular stress. However, it is not known if, or to what extent, the transcription process itself is affected by aging. In this study, we have investigated how the kinetics of transcription is affected by aging, how such changes can affect mRNA biosynthesis, and the role of these changes in age-related loss of function in the whole organism.

The translocation speed of RNA polymerase II (Pol-II) during transcription can be monitored using total RNA sequencing (RNA-seq), because the distribution of reads in introns is affected by the elongation speed of Pol-II. Co-transcriptional splicing results in a characteristic saw-tooth pattern of the read coverage, observable from total RNA-seq or nascent RNA-seq measurements (*11*, *12*). The read coverage generally decreases 5' to 3' along an intron and the extent of this decrease depends on Pol-II speed: the faster the elongation, the shallower the slope (*13-15*), i.e. fast elongation of Pol-II results in fewer nascent transcripts interrupted inside introns at the moment when the cells are lysed (Fig. 1, A and B). Thus, by quantifying the gradient of read coverage along an intron it is possible to

bioRxiv preprint doi: https://doi.org/10.1101/719864; this version posted August 8, 2019. The copyright holder for this preprint (which was not certified by peer review) is the author/funder, who has granted bioRxiv a license to display the preprint in perpetuity. It is made available under aCC-BY-NC-ND 4.0 International license.

determine Pol-II elongation speeds at the resolution of single introns (Fig. 1, A and B). Note that this measure is only weakly associated with the expression level of the transcript (*16*) (Fig. S1).

To monitor the kinetics of transcription, we quantified the distribution of intronic reads resulting from RNA sequencing in five animal species: the worm *C. elegans*, the fruit fly *D. melanogaster*, the mouse *M. musculus*, the rat *R. norvegicus* (*17*), and human *H. sapiens*, at different adult ages (Extended Data Table 1, see Methods). Samples were taken from diverse mammalian tissues (brain, liver, kidney, whole blood), from fly brains, and whole worms. Human samples originated from whole blood (healthy donors, age 21-70), fibroblasts from an individual with a progeria syndrome compared to an age- and sex-matched healthy control, and from two human cell lines (IMR90, HUVEC) that were driven into replicative senescence. After filtering, we obtained between 546 and 14,593 introns that passed the quality criteria for reliable Pol-II speed quantification (see Methods). Interestingly, we observed an increase of average Pol-II rates with age for all five species and all tissue types examined (Fig. 1C and Fig. S2). The average effect sizes varied from +33 *bp/min* in mouse kidney to +146 *bp/min* in rat liver. To address whether the lifespan-extending interventions inhibition of insulin/insulin-like growth factor signaling (IIS) and dietary restriction affected Pol-II speeds, we sequenced samples from IIS mutants, using *daf-2* mutant worms at day 14 and fly brains from *dilp2-3,5* mutants at day 30 and day 50, and hypothalamus from aged wild type and *IRS1* null mice. Further, we sequenced samples from kidney and liver of dietary restricted (DR) and *ad libitum* fed mice. In all comparisons, the lifespan-extending interventions resulted in a significant reduction of Pol-II speed. Pol-II elongation speed thus increased with age across a wide range of animal species and tissues, and this increase was at least partially reverted under various lifespan-extending conditions.

bioRxiv preprint doi: https://doi.org/10.1101/719864; this version posted August 8, 2019. The copyright holder for this preprint (which was not certified by peer review) is the author/funder, who has granted bioRxiv a license to display the preprint in perpetuity. It is made available under aCC-BY-NC-ND 4.0 International license.

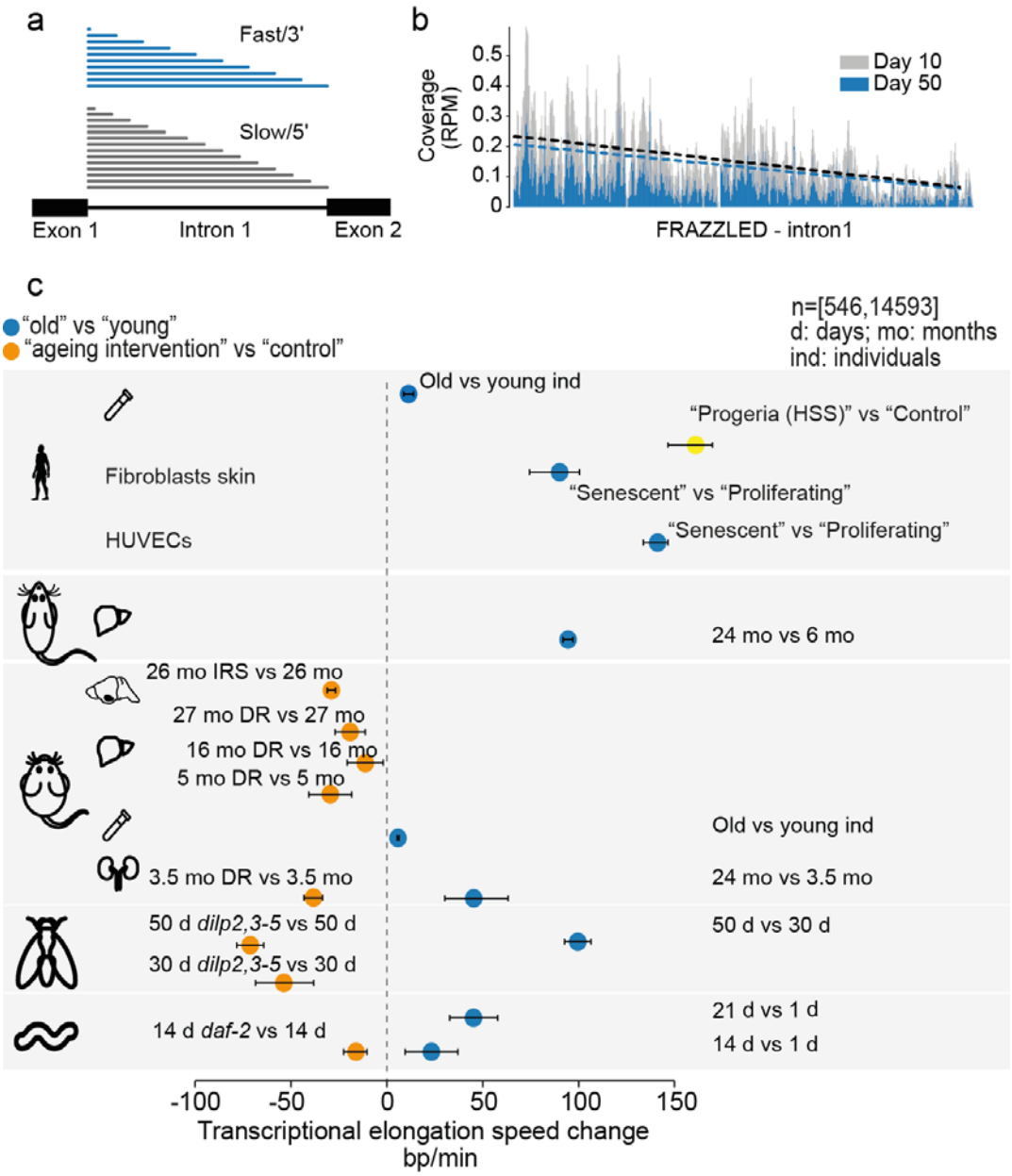

Fig. 1: Pol-II elongation rate increases with age and is slowed-down by reduced insulin signaling and dietary restriction (DR) in multiple species. (A) Schematic representation of read coverage along introns in total RNA seq. Intronic reads represent transcriptional production at a given point in time. A shallower slope of the read distribution is a consequence of increased Pol-II elongation speed. (**B**) Exemplary read distribution in the FRAZZLED intron 1 with coverage in RPM for *D. melanogaster* at age day 10 (grey) and day 50 (blue). (**C**) Change of average Pol-II elongation rates (*bp/min*) in worm (whole body), fruit fly (brains), mouse (kidney, liver, hypothalamus, blood), rat (liver), human blood, and human cell culture (Fibroblast skin cells derived from a HSS progeria patient compared to a healthy control; HUVECs: umbilical vein endothelial; IMR90: fetal lung). Error bars show median variation ±95% confidence interval. All changes of average elongation speeds are significantly different from zero ($P < 0.001$; paired Wilcoxon rank test). Number of introns considered (*n*) ranged from 546 to 14593.

bioRxiv preprint doi: https://doi.org/10.1101/719864; this version posted August 8, 2019. The copyright holder for this preprint (which was not certified by peer review) is the author/funder, who has granted bioRxiv a license to display the preprint in perpetuity. It is made available under aCC-BY-NC-ND 4.0 International license.

To determine whether genes with particular functions were more strongly affected by Pol-II speed changes, we performed gene set enrichment analysis on the 200 genes with the highest increase in Pol-II speed during aging in worms, fly brains, mouse kidneys and livers and rat livers. Only very generic functional classes, such as metabolic activity, were consistently enriched across three or more species (see Methods and Fig. S3). Thus, no specific cellular process seemed to be affected consistently across species and tissues. Next, we examined age-associated gene expression changes of transcription elongation regulators. We observed that some regulators (PAF1, THOC1) were consistently down-regulated across species during aging (Fig. S4), which was also confirmed using gene set enrichment analysis (Fig. S5). These findings suggest a potential cellular response to unwanted variation of transcriptional elongation speed.

To determine if changes in Pol-II elongation speed were causally involved in in the aging process, we used genetically modified worm and fly strains carrying point mutations in a Pol-II main subunit that reduce its elongation speed (*C. elegans, ama-1* (m322) mutant (*18*) ; *D. melanogaster*, *RpII215*^{C4} mutant (*19*)). To confirm that these mutants reduced Pol-II elongation speed, we sequenced total RNA from wild type and slow Pol-II mutant worms (whole body at day 14) and fly heads, at day 10 and day 50. Estimates of transcription elongation rate confirmed the effects of the Pol-II slow mutants: average Pol-II speeds were lower in *C. elegans ama-1* (m322) by -78 *bp/min* and in *D. melanogaster RpII215*^{C4} by -70 *bp/min* (Fig. 3A). To determine if Pol-II elongation rate, with its associated maintenance of transcriptional fidelity, also affected aging of the whole organism, we measured effects on lifespan. Slowing down Pol-II resulted in increased lifespans in both the worm and fruit fly (median lifespan increase: *C. elegans*: ~20 %; *D. melanogaster*: ~10 %; Fig. 2B and Fig. S6). Further, mutant worms had a higher pharyngeal pumping rate at older age compared to wild

bioRxiv preprint doi: https://doi.org/10.1101/719864; this version posted August 8, 2019. The copyright holder for this preprint (which was not certified by peer review) is the author/funder, who has granted bioRxiv a license to display the preprint in perpetuity. It is made available under aCC-BY-NC-ND 4.0 International license.

type worms, suggesting that healthspan was also extended by slowing down Pol-II elongation speed (Fig. S7).

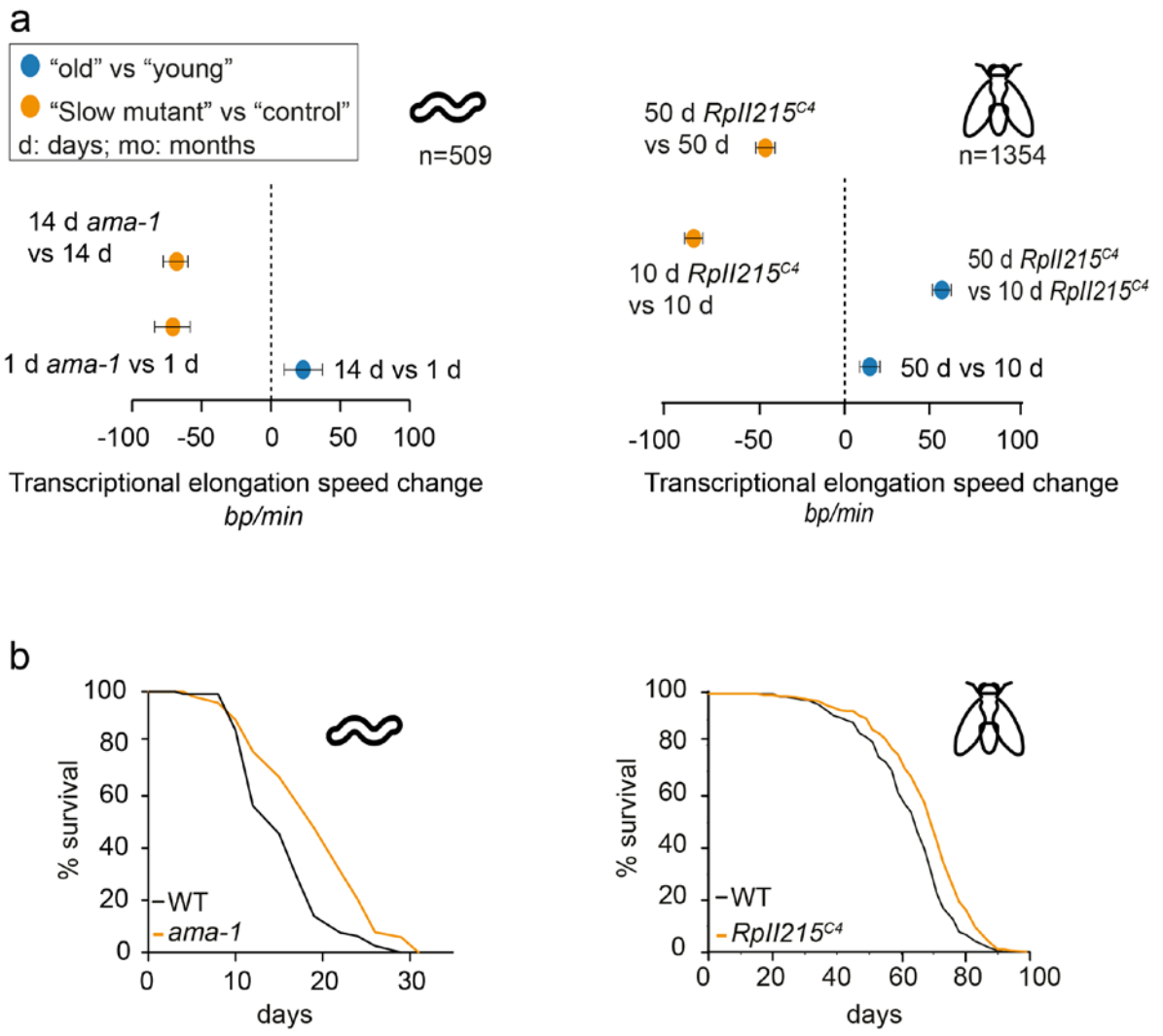

Fig. 2: Molecular and lifespan effects of reduced Pol-II elongation speed in *C. elegans and D. melanogaster*. (A) Differences of average Pol-II elongation speeds between Pol-II mutant and wild-type worms (**left**) and flies (**right**), and changes of average Pol-II elongation speeds with age in flies (right). Error bars show median variation ±95% confidence interval. All average changes of Pol-II elongation speeds are significantly different from zero ($P < 0.001$; paired Wilcoxon rank test). **(B)** Survival curves of animals with *RpII215*^{C4} mutation and wild-type controls for worms (**left, replicate 1**) and flies (**right, averaged survival curve**) (worms 4 replicates, See Fig. S4; flies 3 replicates). Animals with slow Pol-II have a significantly increased lifespan (+20 % and +10 % median lifespan increase for *C. elegans* (n=120, $P < 0.001$, log rank test) and *D. melanogaster* (n=220, $P < 0.001$, log rank test), respectively).

bioRxiv preprint doi: https://doi.org/10.1101/719864; this version posted August 8, 2019. The copyright holder for this preprint (which was not certified by peer review) is the author/funder, who has granted bioRxiv a license to display the preprint in perpetuity. It is made available under aCC-BY-NC-ND 4.0 International license.

An optimal elongation rate is required for fidelity of alternative splicing (*20*, *21*): for some exons, slow elongation favors weak splice sites, leading to exon inclusion, while these are skipped during fast elongation (*5*, *22*, *23*). Further, a faster elongation rate can promote intron retention, leading to degradation of the transcript via nonsense-mediated decay (NMD) (*24*) or inactivation of tumor suppressor effects (*25*). Therefore, we next quantified changes in splicing efficiency as the fraction of spliced reads from all reads aligning over a given splice site (*26*). In most datasets from total RNA and nascent RNA sequencing we observed an increase of the spliced exon junctions relative to unspliced junctions during aging and a reduction of the percent spliced junctions under lifespan-extending conditions (Fig. S8. Thus, surprisingly we observed more spliced transcripts under conditions when Pol-II speed is accelerated, i.e. greater splicing efficiency. In the case of co-transcriptional splicing, the removal of lariats depends on the position of Pol-II in the gene (*27*, *28*). In this context, our data therefore suggests that accelerated transcription shortens the time to splicing, which reduces the effective half-life of lariats.

Accelerated transcription and splicing carries the risk of increasing the number or erroneous splicing events, which in turn has been associated with advancing age and shortened lifespan (*29*-*32*). It is non-trivial to tell if a specific splice isoform is the product of erroneous splicing or if it was created in response to a specific signal. Simply checking if an observed isoform is reported in some genome annotation database is problematic for multiple reasons. On the one hand, such databases were mostly created using data from young or embryonic animals. Thus, the detected isoform may be functionally relevant in old animals, but not reported in such database. On the other hand, an annotated isoform might be the result of erroneous splicing if otherwise it should not be expressed in that particular age class or cellular context. Hence, we based our analysis on the notion that extremely rare isoforms (rare with respect to all other isoforms of the same gene in the same sample) are more likely erroneous than are

bioRxiv preprint doi: https://doi.org/10.1101/719864; this version posted August 8, 2019. The copyright holder for this preprint (which was not certified by peer review) is the author/funder, who has granted bioRxiv a license to display the preprint in perpetuity. It is made available under aCC-BY-NC-ND 4.0 International license.

frequent isoforms (*33*, *34*). We defined rare splicing events as all exon-exon junctions that are supported by fewer or equal to 0.07 percent of all junctions detected for a given gene (*33*). Then, the gene-specific fraction of rare exon-exon junctions was computed as the number of rare exon-exon junctions divided by the total number of detected exon-exon junctions from that gene. Indeed, we observed that these rare exon-exon junctions often resulted from exon skipping or from the usage of cryptic splice sites (Fig. S9a). We observed an increase of the average fraction of rare splicing events during aging across all five species and a reversion of this effect under most lifespan-extending conditions (Fig. 3, Fig. S10). Importantly, the fraction of rare splicing events was also reduced in old flies and worms with mutations slowing down Pol-II (Fig. 3). Further, we noticed that genes with increased Pol-II elongation speed had on average larger fractions of rare isoforms than genes with reduced speed (Fig. S9b).

Another potential indicator of erroneous splicing is the increased formation of circular RNAs (circRNAs) (*35*, *36*). Increased Pol-II elongation speed has previously been associated with increased expression of circRNAs (*37*), i.e. back-spliced transcripts with a covalent binding of their 5' and 3' ends (*38*). We quantified the fraction of circRNAs as the number of back-spliced fragments normalized by the sum of back-spliced fragments and linearly spliced fragments. During aging (old *versus* young) we observed either increased or unchanged average circRNA fractions (Fig. S11). In contrast, reducing Pol-II speed reduced circRNA formation, thereby maintaining the proper splicing of genes hosting circRNAs. Thus, our data suggests that faster Pol-II elongation resulted in an increase of circRNA formation, which lead to a global increase of exon skipping for genes hosting circular RNAs. Taken together, these findings suggest that an age-associated acceleration of transcription and splicing leads to increased splicing noise with impact on lifespan.

bioRxiv preprint doi: https://doi.org/10.1101/719864; this version posted August 8, 2019. The copyright holder for this preprint (which was not certified by peer review) is the author/funder, who has granted bioRxiv a license to display the preprint in perpetuity. It is made available under aCC-BY-NC-ND 4.0 International license.

Interestingly, specific genes with important functions in aging-associated phenotypes were consistently affected by the changes in Pol-II elongation speed and splicing outcome in multiple species. For example, we observed an increase in transcriptional elongation speed in the DNA repair gene PARP1 during aging in human cell lines (IMR90), mouse kidney, rat liver, and fly brain (in the remaining samples the elongation speed in PARP1 could not be quantified due to insufficient read coverage in the introns). Interestingly, we observed a reduction of the major PARP1 isoform in older mammals/senescent human cells along with an increase of truncated isoforms containing only parts of the protein (Fig. S12, PARP1 and ITPR1 isoform fraction change during aging). Thus, the age-associated increase in elongation speed of PARP1 coincides with the expression of non-functional isoforms (*39*).

Increased Pol-II elongation speed can lead to elevated transcriptional errors, because the proofreading capacity of Pol-II is reduced (*8*). To explore the potential impact of transcriptional elongation on transcript quality beyond splicing, we measured the number of mismatches in aligned reads for each gene normalized by its respective expression level. During this counting, we excluded mismatches that were likely due to genome variants or other artifacts (see Methods for details). We observed that the average fraction of mismatches increased with age and that it decreased under most lifespan-extending treatment (Fig S13). Consistent with prior findings (*8*), slow Pol-II mutants exhibited reduced numbers of mismatches compared to their wild-type controls in 3 out 4 comparisons. Hence, our findings suggest that increased Pol-II elongation speed results in increased errors in transcripts, presumably due to a reduced proofreading capacity (*8*).

bioRxiv preprint doi: https://doi.org/10.1101/719864; this version posted August 8, 2019. The copyright holder for this preprint (which was not certified by peer review) is the author/funder, who has granted bioRxiv a license to display the preprint in perpetuity. It is made available under aCC-BY-NC-ND 4.0 International license.

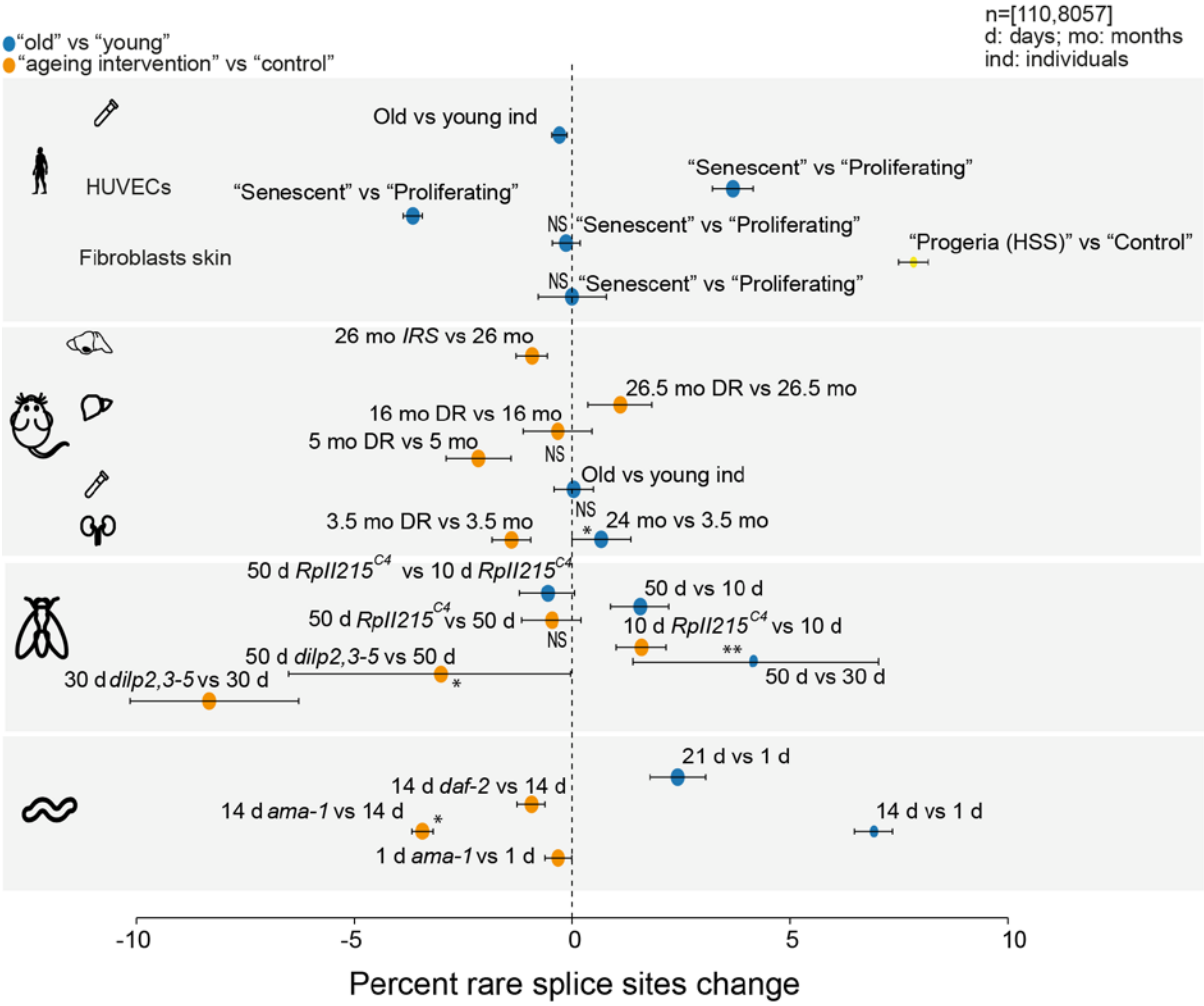

Fig. 3: Percent of rare splicing events mostly increases with age and goes down upon lifespan-extending treatments. Average percent changes of rare splice events (<= 0.07 percent of total gene expression) with age (blue) and upon lifespan extending treatments (orange). Error bars show median variation ±95% confidence interval. All changes of average rare splice events are significantly different from zero ($P < 0.001$; paired Wilcoxon rank test), except those labeled NS (not significant), **$P < 0.01$, *: $P < 0.05$. Number of genes considered (*n*) ranged from 110 to 8057.

Finally, we explored alterations in chromatin structure as a potential cause of age-associated changes of Pol-II elongation speed. Nucleosome positioning along the DNA fiber is known to affect both Pol-II elongation speed and splicing efficiency (*15*, *40-42*). Furthermore, older eukaryotic cells display reduced nucleosomal density in chromatin and "noisier" core nucleosome positioning (*43*, *44*). Thus, age-associated changes in chromatin structure might contribute to the changes in Pol-II elongation speed and splicing efficiency that we observed

bioRxiv preprint doi: https://doi.org/10.1101/719864; this version posted August 8, 2019. The copyright holder for this preprint (which was not certified by peer review) is the author/funder, who has granted bioRxiv a license to display the preprint in perpetuity. It is made available under aCC-BY-NC-ND 4.0 International license.

here. To probe this hypothesis, we performed micrococcal nuclease (MNase) digestion of chromatin from early (proliferating) and late-passage (senescent) human IMR90 cells, followed by ~400 million paired-end read sequencing of the mononucleosomal DNA fragments (MNase-seq). Following mapping, we explored changes in nucleosome occupancy and positioning over exons and exon-intron boundaries (*45*). We observed that nucleosome peaks moved away from exon centers and from exon-intron boundaries in senescent versus proliferating cells (Fig. 4, A and B). In addition, we quantified 'fuzziness', which reflects the precision of nucleosome positioning in a given MNase-seq dataset (see Methods). We also used the distance between nucleosome summits as a measure of the nucleosome position regularity (*46*, *47*). Both measures changed significantly in senescent cells (Fig. 4, C and D): the average fuzziness was increased (in exons and introns) and the distances between nucleosome peaks became more variable in senescent cells. Finally, we compared changes in Pol-II elongation speed to fuzziness and distance. Introns showing faster transcriptional elongation exhibited greater changes in nucleosome positioning precision and regularity than introns with reduced elongation speed (Fig. 4, E and F). Importantly, whereas the average distance between nucleosomes did not differ between 'fast' and 'slow' introns, there was a significant increase of the variability of nucleosome distances in introns with increased elongation speed (Fig. 4F). These results suggest that reduced precision in the assembly of the chromatin fiber may contribute to changes in Pol-II speed and splicing fidelity (*40*, *44*, *48*) .

We have found a consistent increase in average Pol-II elongation speed with age across four animal models and three human cell lines, and we could revert this trend by employing lifespan-extending treatments. We observed consistent changes in splicing and transcript quality that correlated with Pol-II elongation speed changes and which likely contribute to

bioRxiv preprint doi: https://doi.org/10.1101/719864; this version posted August 8, 2019. The copyright holder for this preprint (which was not certified by peer review) is the author/funder, who has granted bioRxiv a license to display the preprint in perpetuity. It is made available under aCC-BY-NC-ND 4.0 International license.

age-associated phenotypes. Although the average changes were significant in all species, they remained small in absolute terms. This is expected as drastic genome-wide changes of RNA biosynthesis would likely lead to an immediate and complete loss of cellular functions and thus early death. Instead, here we are monitoring the gradual reduction of cellular fitness that is characteristic for normal aging. Importantly, we were able to improve splicing quality and lifespan in two species by reducing the Pol-II elongation speed. Thus, despite being small in magnitude, the effects are clearly biologically relevant for lifespan. Whereas our work establishes altered mRNA biosynthesis as a mechanism driving aging, we still lack a complete understanding of the molecular mechanisms driving Pol-II elongation speed changes.

Our work established that the elongation speed of Pol-II as an important contributor to molecular and physiological traits with implications beyond aging. Mis-regulation of transcriptional elongation factors reduces cellular and organismal fitness and may therefore contribute to disease phenotypes (*49*). Taken together, the data presented here reveal a new molecular mechanism contributing to aging and serve as a template for assessing the fidelity of cellular machinery during aging and disease.

bioRxiv preprint doi: https://doi.org/10.1101/719864; this version posted August 8, 2019. The copyright holder for this preprint (which was not certified by peer review) is the author/funder, who has granted bioRxiv a license to display the preprint in perpetuity. It is made available under aCC-BY-NC-ND 4.0 International license.

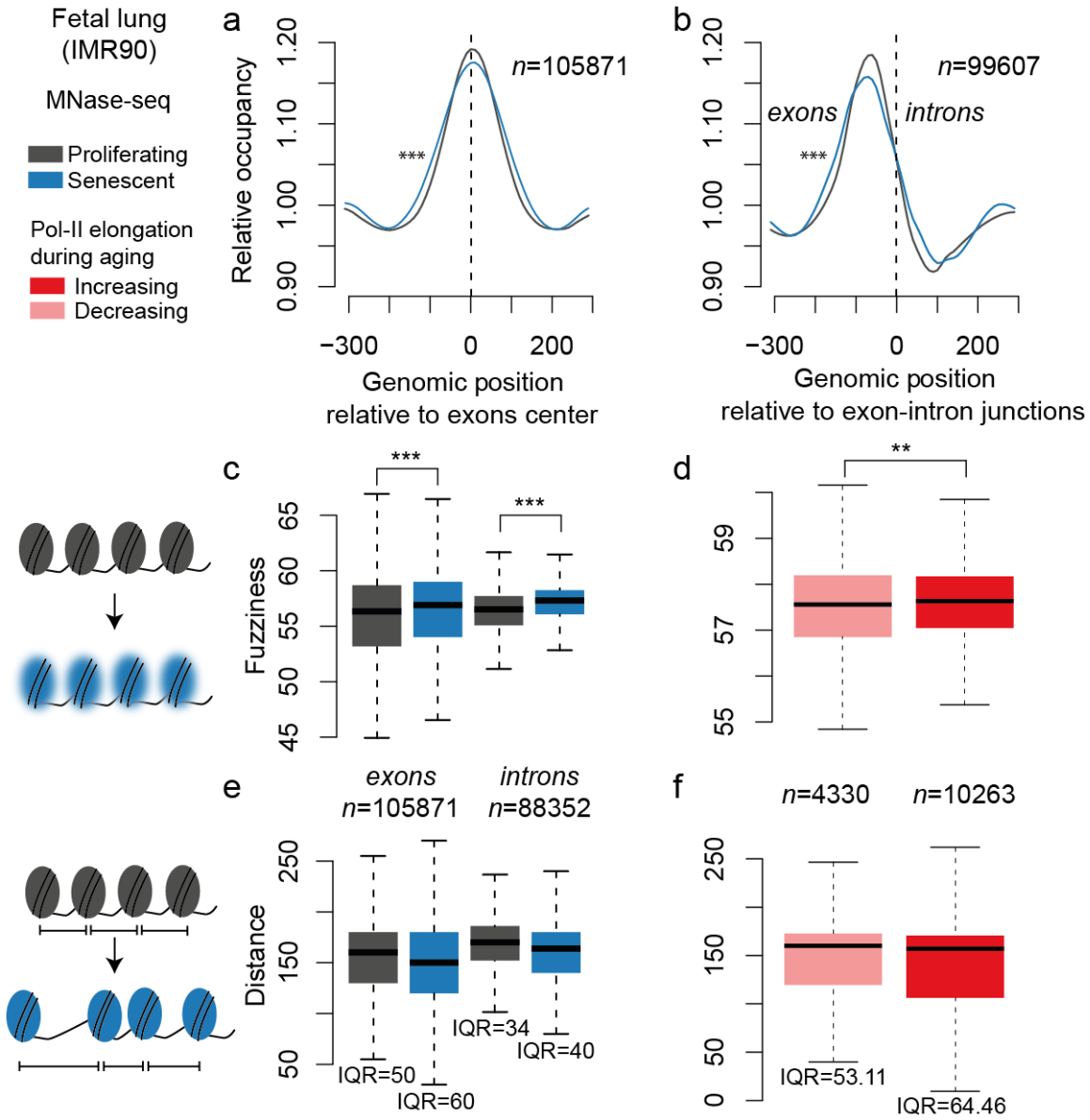

Fig. 4: Profiling of nucleosome positioning in human cell models. Meta-analysis profile of nucleosome occupancy on DNA (non-stranded) over (**A**) exon centers and (**B**) at exon-intron boundaries. Distribution of nucleosome fuzziness for (**C**) proliferating (grey) and senescent (dark blue) cells, and (**D**) increasing (dark red) and decreasing (light red) Pol-II speed. Statistical significance from difference in distribution indicated by asterisks (*** $P < 0.001$, ** $P < 0.01$, un-paired Wilcoxon rank test) for **C**, **D.** Distributions of distances between nucleosome summits for (**E**) proliferating (grey) and senescent (dark blue), and (**F**) increasing (dark red) and decreasing (light red) Pol-II speed. **E:** nucleosomes are distinguished based on whether they are in exons (left) or introns (right). Interquartile range (IQR) is a measure of statistical dispersion **E, F**.

bioRxiv preprint doi: https://doi.org/10.1101/719864; this version posted August 8, 2019. The copyright holder for this preprint (which was not certified by peer review) is the author/funder, who has granted bioRxiv a license to display the preprint in perpetuity. It is made available under aCC-BY-NC-ND 4.0 International license.

Methods

Worm strains and demography assays

Nematodes were cultured using standard techniques at 20 ° C on NGM agar plates and were fed with *E.coli* strain OP50. *DR786* strain carrying the *ama-1(m322)* IV mutation in the large subunit of Pol-II (RBP1), which confers alpha-amanitin resistance, was obtained from Caenorhabditis Genetics Center (CGC) (*50, 51*). DR786 strain was then outcrossed into *N2 wild type* strain 4 times and mutation was confirmed by sequencing. 5'-3' AGAAGGTCACACAATCGGAATC primer was used for sequencing. For each genotype, minimum of 120 age-matched day 1 young adults were scored every other day for survival and transferred to new plates to avoid starvation and carry-over progeny. Worms undergoing internal hatching, protruding vulva or crawling off the plates were censored. Demography experiments were repeated multiple times. For all experiments, genotypes were blinded. Statistical analyses were performed using Mantel-Cox log rank method.

Fly strains and fly maintenance

The *RpII215*^{C4} fly strain (RRID:BDSC_3663), which carries a single point mutation (R741H) in the gene encoding the *Drosophila* RNA polymerase II 215kD subunit (RBP1) was received from the Bloomington *Drosophila* Stock Center (Bloomington, Indiana, USA). Flies carrying the *RpII215*^{C4} allele (*52*) are homozygous viable but show a reduced transcription elongation rate (*19*). *RpII215*^{C4} mutants were backcrossed for 6 generations into the outbred *white Dahomey (wDah)* wild type strain. A PCR screening strategy was used to follow the *RpII215*^{C4} allele during backcrossing. Therefore, genomic DNA from individual flies was used as a template for a PCR reaction with primers SOL1064 (CCGGATCACTGCTGCATATTTGTT) and SOL1047 (CCGCGCGACTCAGGACCAT). The 582 *bp* PCR product was restricted with BspHI, which specifically cuts only in the

bioRxiv preprint doi: https://doi.org/10.1101/719864; this version posted August 8, 2019. The copyright holder for this preprint (which was not certified by peer review) is the author/funder, who has granted bioRxiv a license to display the preprint in perpetuity. It is made available under aCC-BY-NC-ND 4.0 International license.

RpII215^{C4} allele resulting in two bands of 281 *bp* and 300 *bp*. At least 20 individual positive female flies were used for each backcrossing round. Long-lived insulin mutant flies, which lack three of the seven *Drosophila* insulin-like peptides, *dilp2-3,5* mutants (RRID:BDSC_30889) (*53*) were also backcrossed into the *wDah* strain, which was used as wild type control in all fly experiments. Flies were maintained and experiments were conducted on 1,0 SY-A medium at 25°C and 65% humidity on a 12L:12D cycle (*53*).

Pharyngeal pumping rate

Synchronized wild type and ama-1 (m322) animals were placed on regular NGM plates seeded with OP50 bacteria on day1 and day8 adulthood and number of pharyngeal pumping rate was assessed by observing the number of pharyngeal contractions during a 10sec interval using dissecting microscope and Leica Application Suite X imaging software. Pharyngeal pumping rate was then adjusted for number of pharyngeal pumping per minute. Animals that displayed bursting, internal hatching and death were excluded from the experiments. Experiments were repeated three independent times in a blinded fashion, scoring minimum of 15 randomly selected animals per genotype and time point for each experiment. One-way Anova with Tukey's multiple comparison test was used for statistical significance testing. p-value < 0.0001****, error bars represent standard deviation.

Fly lifespan assays

For lifespan assays fly eggs of homozygous parental flies were collected during a 12 h time window and the same volume of embryos was transferred to each rearing bottle ensuring standard larval density. Flies that eclosed during a 12 h time window were transferred to fresh bottles and were allowed to mate for 48h. Subsequently, flies were sorted under brief CO_2 anesthesia and transferred to vials. Flies were maintained at a density of 15 flies per vial and were transferred to fresh vials every two to three days and the number of dead flies was

bioRxiv preprint doi: https://doi.org/10.1101/719864; this version posted August 8, 2019. The copyright holder for this preprint (which was not certified by peer review) is the author/funder, who has granted bioRxiv a license to display the preprint in perpetuity. It is made available under aCC-BY-NC-ND 4.0 International license.

counted. Lifespan data were recorded using Excel and were subjected to survival analysis (log rank test) and presented as survival curves.

Mouse maintenance and dietary restriction protocol

The DR study was performed in accordance with the recommendations and guideline of the Federation of the European Laboratory Animal Science Association (FELASA), with all protocols approved by the Landesamt für Natur, Umwelt und Verbraucherschutz, Nordrhein-Westfalen, Germany. Details of the mouse liver DR protocol have been published previously (Hahn et al., 2017). For the mouse kidney, Male *C57BL/6* mice were housed under identical SPF conditions in group cages (5 or fewer animals per cage) at a relative humidity of 50-60% and a 12 hour light and 12 hour dark rhythm. For dietary restriction vs control, 8 week old mice were used. Dietary restriction was applied for 4 weeks. Control mice received food and water ad libitum. Mice were sacrificed at 12 weeks. For comparison of young vs aged mice, 14 week and 96 week old mice were used. Food was obtained from ssniff (Art. V1534-703, Soest, Germany) and Special Diet Services (Witham, UK). The average amount of food consumed by a mouse was determined by daily weighing for a period of two weeks and was on average 4,3 g per day. DR was applied for 4 weeks by feeding 70% of the measured ad libitum amount of food. Water was provided ad libitum. Mice were weighed weekly to monitor weight loss. Neither increased mortality nor morbidity was observed during dietary restriction.

RNA extraction

Wild-type N2 strain, alpha-amanitin resistant *ama-1(m322)* mutants and long-lived insR/IGF signaling mutants, *daf-2*(*e1370*) were sent for RNA-seq. For each genotype, more than 300 aged-matched adult worms at desired time points were collected in Trizol (Thermo Fisher Scientific, USA) in 3 biological replicates. Total RNA was extracted using RNAeasy Mini kit

bioRxiv preprint doi: https://doi.org/10.1101/719864; this version posted August 8, 2019. The copyright holder for this preprint (which was not certified by peer review) is the author/funder, who has granted bioRxiv a license to display the preprint in perpetuity. It is made available under aCC-BY-NC-ND 4.0 International license.

(Qiagen, Hilden, Germany). For fly samples, brains of 30 days and 50 days old *dilp2-3,5* and *wDah* control flies were dissected manually and snap frozen. 10 days and 50 days old *RpII215*^{C4} mutants and *wDah* control flies were snap frozen and fly heads were isolated by vortexing and sieving on dry ice. Total RNA from three biological samples per treatment group was prepared using Trizol Reagent according to the manufacturer's instructions, followed by DNAse treatment with the TURBO DNA-free Kit (Thermo Fisher Scientific). Mouse liver samples were isolated from 5, 16 and 27 months old ad libitum and DR animals, which corresponded to 2, 13 and 24 months of DR treatment, respectively. RNA was isolated by Trizol and DNase-treated. The RNA-seq data for 5 and 27 months old liver DR samples have been published previously (*54*), while the 16 months data are first published here. RNeasy mini Kit and Trizol were used to isolate RNA from snap-frozen kidneys as per manufacturer's instructions. Hypothalamus tissue of long-lived insulin receptor substrate 1 (*IRS1-/-*) knock out mice (*55*) and *C57BL/6* black control animals was dissected manually at the age of 72 weeks. RNA was isolated by Trizol with subsequent DNase treatment. For blood samples globin RNA was removed using GLOBINclear™ Kit, mouse/rat/human, for globin mRNA depletion.

Human cell culture

Human umbilical vein endothelial cells (HUVECs) from pooled donors (Lonza, Cologne, Germany) and Human fetal lung (IMR-90) cells (from two donors) were grown to 80% to 90% confluence in endothelial basal medium 2-MV with supplements (EBM; Lonza) and 5% foetal bovine serum (FBS) and MEM (Sigma-Aldrich) with 20 FBS (Gibco) and 1% non-essential amino acids (Sigma-Aldrich) for HUVECs and IMR-90 respectively.

bioRxiv preprint doi: https://doi.org/10.1101/719864; this version posted August 8, 2019. The copyright holder for this preprint (which was not certified by peer review) is the author/funder, who has granted bioRxiv a license to display the preprint in perpetuity. It is made available under aCC-BY-NC-ND 4.0 International license.

Total RNA and nascent RNA sequencing

From 1 µg input of total RNA, ribosomal RNA was removed using the Ribo-Zero Human/Mouse/Rat kit (Illumina). Sequencing libraries were generated according to the TruSeq stranded total RNA (Illumina) protocol. To generate the final cDNA library, products were purified and amplified by PCR for 15 cycles. After validation and quantification of the library on an Agilent 2100 Bioanalyzer, equimolar amounts of libraries were pooled. Pools of 5 libraries were sequenced per lane on an Illumina HiSeq 4000 sequencer. For a description of all the RNA-seq datasets used in this study see Extended Data Table 1. The same protocol was used to sequence cDNA libraries from human cell "factory" RNA, which was isolated as described previously (*56*).

RNA-seq alignments and gene expression analysis

Raw reads were trimmed with trimmomatic version 0.33 (*57*) using parameters 'ILLUMINACLIP:./Trimmomatic-0.33/adapters/TruSeq3-PE.fa:2:30:10 LEADING:3 TRAILING:3 SLIDINGWINDOW:4:15 MINLEN:45' for paired-end datasets and 'ILLUMINACLIP:./Trimmomatic-0.33/adapters/TruSeq3-SE.fa:2:30:10 LEADING:3 TRAILING:3 SLIDINGWINDOW:4:15 MINLEN:45' for single-end datasets. Alignment was performed with STAR version 2.5.1b (*58*) using the following parameters: '--outFilterType BySJout --outWigNorm None' on the genome version mm10, rn5, hg19, dm6, ce5 for *M. musculus, R. norvegicus, H. sapiens, D. melanogaster, C. elegans*, respectively. We estimated transcript counts using Kallisto version 0.42.5 for each sample. To determine differentially expressed genes we used DESeq2 version 1.8.2 (*59*) with RUVr normalization version 1.6.2 (*60*). For the differential analysis of transcriptional elongation regulators, we downloaded the list of positive and negative regulators from the GSEA/MSigDB (*61*). Gene ontology (GO) term enrichment analysis of differentially expressed genes or genes with

bioRxiv preprint doi: https://doi.org/10.1101/719864; this version posted August 8, 2019. The copyright holder for this preprint (which was not certified by peer review) is the author/funder, who has granted bioRxiv a license to display the preprint in perpetuity. It is made available under aCC-BY-NC-ND 4.0 International license.

increased RNA-Pol-II elongation speed was carried out using TopGO version 2.20.0. For GO enrichment analysis of differentially expressed genes, we identified 4784 genes as evolutionarily conserved from each species of our study to humans: genes were either direct orthologues (one2one) or fusion genes (one2many) of *H. sapiens* were retrieved from ENSEMBL database using biomaRt 2.24.1 (*62*). Using our 4784 genes evolutionary conserved, we further divided into consistently up-regulated or down-regulated genes across species during aging or 'aging intervention' (as target set for GO enrichment: aging up-regulated: 92 genes; aging down-regulated: 71; 'aging intervention' up-regulated: 164 genes; 'aging intervention' down-regulated: 473 genes; as background set 4784 orthologue genes between *R. norvegicus*, *M. musculus*, *D. melanogaster*, *C. elegans*, and *H. hsapiens*). For GO enrichment analysis of genes harboring increasing Pol-II speed, we used as target set the top 200 or 300 genes with an increase in Pol-II speed change for each species. For circular RNA, we aligned the read using STAR version 2.5.1b (*58*) with the following parameters:' --chimSegmentMin 15 --outSJfilterOverhangMin 15 15 15 15 --alignSJoverhangMin 15 --alignSJDBoverhangMin 15 --seedSearchStartLmax 30 --outFilterMultimapNmax 20 --outFilterScoreMin 1 --outFilterMatchNmin 1 --outFilterMismatchNmax 2 --chimScoreMin 15 --chimScoreSeparation 10 --chimJunctionOverhangMin 15'. We then extracted back spliced reads from STAR chimeric output file and normalized the number of back spliced reads by the sum of back spliced (BS_i) and spliced reads from linear transcripts ($S1_i$, $S2_i$) for an exon *i* (*7*):

$$CircRatio_i = \frac{BS_i}{BS_i + \frac{S1_i + S2_i}{2}} * 100$$

Here, $S1_i$ refers to the number of linearly spliced reads at the 5' end of the exon and $S2_i$ refers to the respective number of reads at the 3' end of the exon. Thus, this score quantifies the percent of transcripts from this locus that resulted in circular RNA. Finally, we quantified the

bioRxiv preprint doi: https://doi.org/10.1101/719864; this version posted August 8, 2019. The copyright holder for this preprint (which was not certified by peer review) is the author/funder, who has granted bioRxiv a license to display the preprint in perpetuity. It is made available under aCC-BY-NC-ND 4.0 International license.

significance of the average change in circular RNA formation between two condition using the Wilcoxon rank test.

Definition of intronic regions

All annotation files for this analysis were downloaded from Ensembl website (*64*) using genome version ce10 for *Caenorhabditis elegans*, mm10 for *Mus musculus*, hg19 for *Homo sapiens*, rn5 for *Rattus norvegicus*, dm6 for *Drosophila melanogaster*. The following filtering steps were applied on the intronic ENSEMBL annotation files: First we removed overlapping regions between introns and exons in order to avoid confounding signals due to variation in splicing or transcription initiation and termination. Overlapping introns were merged to remove duplicated regions from the analysis. In the next step we used STAR (*58*) to detect splice junctions and compared them to the intronic regions. Introns with at least 5 split reads bridging the intron (i.e. mapping to the flanking exons) per condition were kept for subsequent analyses. Thereby we ensured a minimum expression level of the spliced transcript. When splice junctions were detected within introns, we further subdivided those introns accordingly. Introns with splice junction straddling were discarded. The above-mentioned steps were performed using Bedtools version 2.22.1 using substract and merge commands. After these filtering steps, the number of usable introns per sample varied between a few hundred (*n*=546, *C. elegans*, total RNA) to over ten thousand (*n*=13,790, *H. sapiens*, nascent-RNA-seq). These large differences resulted from different sequencing depths, sequencing quality (number of usable reads), and from the complexity of the genome (numbers and sizes of introns, number of alternative isoforms, etc.). In order to avoid artifacts due to the different numbers of introns used per sample, we always contrasted the same sets of introns for each comparison of different conditions (e.g. old *versus* young, treatment *versus* control). Further note that certain comparisons were not possible for all species, due to variations in the experimental design. For instance, for mouse kidney only a single time point

bioRxiv preprint doi: https://doi.org/10.1101/719864; this version posted August 8, 2019. The copyright holder for this preprint (which was not certified by peer review) is the author/funder, who has granted bioRxiv a license to display the preprint in perpetuity. It is made available under aCC-BY-NC-ND 4.0 International license.

after lifespan intervention (dietary restriction DR, age 3 months) was available, which prevented a comparison of old versus young DR mice, but allowed comparison with *ad libitum* fed mice of the same young age.

Transcriptional elongation speed

In order to calculate Pol-II speeds we used RNA-seq data obtained from total RNA (*65*) and nascent RNA (*56, 66*) enrichment. In contrast to the widely used polyA enrichment method (*67*), which primarily captures mature, spliced mRNAs and is therefore not suitable to estimate Pol-II speeds based on intronic reads, these methods yield sufficient intronic coverage to quantify elongation rates. To analyze the distribution of intronic reads between conditions, we devised a score for each intron. We fitted the read gradient (slope) along each of selected introns (5'->3'; see above for the filtering criteria). Note that the intron gradient is not influenced by exonucleolytic degradation of excised intron lariats (*68*) and that this measure is only weakly associated with the expression level of the transcript (*16*) (Fig. S1).

In order to transform slopes to Pol-II elongation speed we used the following formalism. We assume an intron of length L and we assume that at steady state a constant number of polymerases is initiating and the same number of polymerases is terminating at the end of the intron; i.e. we assume that premature termination inside the intron can be ignored. Polymerases are progressing at a common speed of k [*bp/min*]. The average time that it takes a polymerase to traverse the whole intron is hence

$$\Delta t = L/k$$

Transcription is initiated at a rate of n polymerases per unit time [*1/min*]. Hence, the number of polymerases N initiating during Δt is:

$$N = \Delta t \times n$$

bioRxiv preprint doi: https://doi.org/10.1101/719864; this version posted August 8, 2019. The copyright holder for this preprint (which was not certified by peer review) is the author/funder, who has granted bioRxiv a license to display the preprint in perpetuity. It is made available under aCC-BY-NC-ND 4.0 International license.

The slope s is the number of transcripts after the distance L minus the number of transcripts at the beginning divided by the length of the intron:

$$s = \frac{0 - N}{L} = \frac{-\Delta t \times n}{L} = \frac{-\frac{L}{k} \cdot n}{L} = \frac{-n}{k}$$

and thus the speed k can be computed from the slope as:

$$k = \frac{-n}{s}$$

Hence, slope and speed are inversely related and the speed depends also on the initiation rate (i.e. the expression rate). However, we observed empirically only a small dependency between expression and slope (*16*) (Fig. S1).

To validate our estimates of Pol-II speeds we compared our data with experimental values estimated via GRO-seq (15) and tiling microarray data (11). There was a significant correlation (GRO-seq: R=0.38, p-value=4e-5, compared to time point 25-50 min see Jonkers et al. (15); Tilling array; R=0.99 ,p-value=<2.6e-16 and Fig. S14) between our data and experimentally measured transcriptional elongation values. Thus, we used this model in order to convert our intronic slopes into Pol-II speeds in base pair per minute (bp/min). Note that this conversion to bp/min was done solely to convert the slopes to physically interpretable units and it has no influence on any of our statistical analyses. Further, for human cell lines our transcriptional elongation average estimate ranged from 3.0 to 4.3 kb/min depending on tissues and stage (proliferating or senescent) a result in the same order of magnitude as previously obtained average speed estimates (69). Finally, we noted that our Pol-II speed estimates for different introns of the same gene were more similar than Pol-II speed estimates for random pairs of introns, implying that gene-specific factors or local chromatin structure influence Pol-II speed (Fig. S15).

bioRxiv preprint doi: https://doi.org/10.1101/719864; this version posted August 8, 2019. The copyright holder for this preprint (which was not certified by peer review) is the author/funder, who has granted bioRxiv a license to display the preprint in perpetuity. It is made available under aCC-BY-NC-ND 4.0 International license.

Mismatches detection

To avoid detection RNA editing or DNA damage we only considered genomic position with only 1 mismatch detected. Since young and old samples were always handled together, we can exclude that consistent differences in the number of mismatches are due to technical biases. The fraction of RNA editing events is generally relatively low and not expected to globally increase with age (*70*) .

MNase-seq sample preparation

Mononucleosomal DNA from proliferating and senescent IMR-90 cells (from two donors) were prepared and sequenced on a Illumina HiSeq4000 platform as previously described (*71*).

MNase-seq analysis

We used DANPOS (*72*) with default parameters to calculate the fuzziness (as the average peak width, where 'width' was quantified as the standard deviation around the peak center (*72*)) and distance between peak summits. Intron and exons annotations were downloaded from UCSC table utilities (*64*) and filtered as described in Definition of intronic regions.

Figures

Species silhouette images where downloaded from phylopic.org. Figures were generated using Adobe Illustrator.

Acknowledgements

RNA-seq data used in this study is available at GEO database under accession numbers: GSE102537 (require token provided with the submission), GSE92486. We acknowledge the Bloomington Drosophila Stock Center for fly stocks and the Max-Planck-Genome-Centre

bioRxiv preprint doi: https://doi.org/10.1101/719864; this version posted August 8, 2019. The copyright holder for this preprint (which was not certified by peer review) is the author/funder, who has granted bioRxiv a license to display the preprint in perpetuity. It is made available under aCC-BY-NC-ND 4.0 International license.

Cologne and the Cologne Center for Genomics for library preparation and sequencing. We thanks Martijn Dollé for providing mice used in the aging kidney experiment. We acknowledge funding from the Max Planck Society, Bundesministerium für Bildung und Forschung Grant SyBACol 0315893A-B (to AB, AA and LP) and the European Research Council under the European Union's Seventh Framework Programme (FP7/2007-2013)/ERC grant agreement number 268739 to LP.

Competing financial interests

The authors declare no competing financial interests.

Corresponding authors

Correspondence to: Argyris Papantonis, Adam Antebi, Linda Partridge, Andreas Beyer

Animal Care (Ethical Statement)

The DR study involving live mice was performed in accordance with the recommendations and guideline of the Federation of the European Laboratory Animal Science Association (FELASA, EU directive 86/609/EEC), with all protocols approved by the Landesamt für Natur, Umwelt und Verbraucherschutz, Nordrhein-Westfalen (LANUV), Germany (reference numbers: 8.87-50.10.37.09.176, 84-02.04.2015.A437, and 84-02.04.2013.A158) and the Netherlands (IACUC in Bilthoven, NIH/NIA 1PO1 AG 17242). The blood samples reference number ethical statement is: 17-362 and the study was registered to the "Deutsches Register Klinischer Studien (DRKS)" and it's identifier is: DRKS00014637.

bioRxiv preprint doi: https://doi.org/10.1101/719864; this version posted August 8, 2019. The copyright holder for this preprint (which was not certified by peer review) is the author/funder, who has granted bioRxiv a license to display the preprint in perpetuity. It is made available under aCC-BY-NC-ND 4.0 International license.

References and notes:

1. *J. E. Darnell, Jr., Variety in the level of gene control in eukaryotic cells. Nature **297**, 365-371 (1982).*

2. *C. Vogel, E. M. Marcotte, Insights into the regulation of protein abundance from proteomic and transcriptomic analyses. Nat Rev Genet **13**, 227-232 (2012).*

3. *Y. Liu, A. Beyer, R. Aebersold, On the Dependency of Cellular Protein Levels on mRNA Abundance. Cell **165**, 535-550 (2016).*

4. *D. L. Bentley, Coupling mRNA processing with transcription in time and space. Nature Reviews Genetics **15**, 163-175 (2014).*

5. *T. Saldi, M. A. Cortazar, R. M. Sheridan, D. L. Bentley, Coupling of RNA Polymerase II Transcription Elongation with Pre-mRNA Splicing. J Mol Biol **428**, 2623-2635 (2016).*

6. *J. W. Conaway, R. C. Conaway, Transcription elongation and human disease. Annu Rev Biochem **68**, 301-319 (1999).*

7. *C. Lopez-Otin, M. A. Blasco, L. Partridge, M. Serrano, G. Kroemer, The hallmarks of aging. Cell **153**, 1194-1217 (2013).*

8. *M. Vermulst et al., Transcription errors induce proteotoxic stress and shorten cellular lifespan. Nat Commun **6**, 8065 (2015).*

9. *S. Rangaraju et al., Suppression of transcriptional drift extends C. elegans lifespan by postponing the onset of mortality. eLife **4 %U** **http://elifesciences.org/lookup/doi/10.7554/eLife.08833**, (2015).*

10. *C. P. Martinez-Jimenez et al., Aging increases cell-to-cell transcriptional variability upon immune stimulation. Science **355**, 1433-1436 (2017).*

11. *Y. Wada et al., A wave of nascent transcription on activated human genes. Proc Natl Acad Sci U S A **106**, 18357-18361 (2009).*

12. *A. Ameur et al., Total RNA sequencing reveals nascent transcription and widespread co-transcriptional splicing in the human brain. Nat Struct Mol Biol **18**, 1435-1440 (2011).*

13. *J. Singh, R. A. Padgett, Rates of in situ transcription and splicing in large human genes. Nat Struct Mol Biol **16**, 1128-1133 (2009).*

14. *G. Fuchs et al., 4sUDRB-seq: measuring genomewide transcriptional elongation rates and initiation frequencies within cells. Genome Biol **15**, R69 (2014).*

15. *I. Jonkers, H. Kwak, J. T. Lis, Genome-wide dynamics of Pol II elongation and its interplay with promoter proximal pausing, chromatin, and exons. eLife **3 %U** **http://elifesciences.org/lookup/doi/10.7554/eLife.02407**, (2014).*

bioRxiv preprint doi: https://doi.org/10.1101/719864; this version posted August 8, 2019. The copyright holder for this preprint (which was not certified by peer review) is the author/funder, who has granted bioRxiv a license to display the preprint in perpetuity. It is made available under aCC-BY-NC-ND 4.0 International license.

16. *A. Veloso et al., Rate of elongation by RNA polymerase II is associated with specific gene features and epigenetic modifications. Genome Research, gr.171405.171113 %U http://genome.cshlp.org/content/early/172014/171404/171408/gr.171405.171113 (2014).*

17. *A. Ori et al., Integrated Transcriptome and Proteome Analyses Reveal Organ-Specific Proteome Deterioration in Old Rats. Cell Systems **1**, 224-237 http://www.sciencedirect.com/science/article/pii/S2405471215001106 (2015).*

18. *T. M. Rogalski, A. M. Bullerjahn, D. L. Riddle, Lethal and amanitin-resistance mutations in the Caenorhabditis elegans ama-1 and ama-2 genes. Genetics **120**, 409-422 (1988).*

19. *Y. Chen, D. Chafin, D. H. Price, A. L. Greenleaf, Drosophila RNA polymerase II mutants that affect transcription elongation. J Biol Chem **271**, 5993-5999 (1996).*

20. *N. Fong et al., Pre-mRNA splicing is facilitated by an optimal RNA polymerase II elongation rate. Genes Dev **28**, 2663-2676 (2014).*

21. *F. C. Oesterreich et al., Splicing of Nascent RNA Coincides with Intron Exit from RNA Polymerase II. Cell **165**, 372-381 (2016).*

22. *M. de la Mata et al., A slow RNA polymerase II affects alternative splicing in vivo. Mol Cell **12**, 525-532 (2003).*

23. *J. Y. Ip et al., Global impact of RNA polymerase II elongation inhibition on alternative splicing regulation. Genome Research **21**, 390-401 http://genome.cshlp.org/content/321/393/390 (2011).*

24. *U. Braunschweig et al., Widespread intron retention in mammals functionally tunes transcriptomes. Genome Res **24**, 1774-1786 (2014).*

25. *H. Jung et al., Intron retention is a widespread mechanism of tumor-suppressor inactivation. Nat Genet **47**, 1242-1248 (2015).*

26. *V. Aslanzadeh, Y. Huang, G. Sanguinetti, J. D. Beggs, Transcription rate strongly affects splicing fidelity and cotranscriptionality in budding yeast. Genome Res **28**, 203-213 (2018).*

27. *L. Herzel, K. Straube, K. M. Neugebauer, Long-read sequencing of nascent RNA reveals coupling among RNA processing events. Genome Res **28**, 1008-1019 (2018).*

28. *H. L. Drexler, K. Choquet, L. S. Churchman, Human co-transcriptional splicing kinetics and coordination revealed by direct nascent RNA sequencing. bioRxiv, 611020 (2019).*

29. *P. Mazin et al., Widespread splicing changes in human brain development and aging. Mol Syst Biol **9**, 633 (2013).*

30. *J. R. Tollervey et al., Analysis of alternative splicing associated with aging and neurodegeneration in the human brain. Genome Research **21**, 1572-1582 %U http://genome.cshlp.org/content/1521/1510/1572 (2011).*

bioRxiv preprint doi: https://doi.org/10.1101/719864; this version posted August 8, 2019. The copyright holder for this preprint (which was not certified by peer review) is the author/funder, who has granted bioRxiv a license to display the preprint in perpetuity. It is made available under aCC-BY-NC-ND 4.0 International license.

31. *B. P. Lee et al., Changes in the expression of splicing factor transcripts and variations in alternative splicing are associated with lifespan in mice and humans. Aging Cell **15**, 903-913 (2016).*

32. *C. Heintz et al., Splicing factor 1 modulates dietary restriction and TORC1 pathway longevity in C. elegans. Nature **541**, 102-106 (2017).*

33. *J. K. Pickrell, A. A. Pai, Y. Gilad, J. K. Pritchard, Noisy splicing drives mRNA isoform diversity in human cells. PLoS Genet **6**, e1001236 (2010).*

34. *N. Stepankiw, M. Raghavan, E. A. Fogarty, A. Grimson, J. A. Pleiss, Widespread alternative and aberrant splicing revealed by lariat sequencing. Nucleic Acids Res **43**, 8488-8501 (2015).*

35. *C. Cocquerelle, B. Mascrez, D. Hetuin, B. Bailleul, Mis-splicing yields circular RNA molecules. FASEB J **7**, 155-160 (1993).*

36. *J. M. Nigro et al., Scrambled exons. Cell **64**, 607-613 (1991).*

37. *Y. Zhang et al., The Biogenesis of Nascent Circular RNAs. Cell Rep **15**, 611-624 (2016).*

38. *X.-O. Zhang et al., Complementary Sequence-Mediated Exon Circularization. Cell **159**, 134-147 http://www.sciencedirect.com/science/article/pii/S0092867414011118 (2014).*

39. *K. Grube, A. Burkle, Poly(ADP-ribose) polymerase activity in mononuclear leukocytes of 13 mammalian species correlates with species-specific life span. Proc Natl Acad Sci U S A **89**, 11759-11763 (1992).*

40. *S. Venkatesh, J. L. Workman, Histone exchange, chromatin structure and the regulation of transcription. Nature Reviews Molecular Cell Biology **16**, 178-189 (2015).*

41. *I. Jonkers, J. T. Lis, Getting up to speed with transcription elongation by RNA polymerase II. Nature Reviews Molecular Cell Biology **16**, 167-177 (2015).*

42. *S. Jimeno-González et al., Proceedings of the National Academy of Sciences of the United States of America **112**, 14840-14845 (2015).*

43. *J. Feser et al., Elevated Histone Expression Promotes Life Span Extension. Molecular Cell **39**, 724-735 http://www.sciencedirect.com/science/article/pii/S1097276510006258 (2010).*

44. *Z. Hu et al., Nucleosome loss leads to global transcriptional up-regulation and genomic instability during yeast aging. Genes & Development **28**, 396-408 http://genesdev.cshlp.org/content/328/394/396 (2014).*

45. *H. Tilgner et al., Nucleosome positioning as a determinant of exon recognition. Nat Struct Mol Biol **16**, 996-1001 (2009).*

bioRxiv preprint doi: https://doi.org/10.1101/719864; this version posted August 8, 2019. The copyright holder for this preprint (which was not certified by peer review) is the author/funder, who has granted bioRxiv a license to display the preprint in perpetuity. It is made available under aCC-BY-NC-ND 4.0 International license.

46. *A. L. Hughes, O. J. Rando, Mechanisms underlying nucleosome positioning in vivo. Annu Rev Biophys **43**, 41-63 (2014).*

47. *K. Struhl, E. Segal, Determinants of nucleosome positioning. Nature Structural & Molecular Biology **20**, 267-273 %* © 2013 Nature Publishing Group, a division of Macmillan Publishers Limited. All Rights Reserved. %U http://www.nature.com/nsmb/journal/v2020/n2013/full/nsmb.2506.html (2013).*

48. *V. Fitz et al., Nucleosomal arrangement affects single-molecule transcription dynamics. Proc Natl Acad Sci U S A, (2016).*

49. *T. E. Miller et al., Transcription elongation factors represent in vivo cancer dependencies in glioblastoma. Nature **547**, 355-359 (2017).*

50. *D. A. Bushnell, P. Cramer, R. D. Kornberg, Structural basis of transcription: alpha-amanitin-RNA polymerase II cocrystal at 2.8 A resolution. Proc Natl Acad Sci U S A **99**, 1218-1222 (2002).*

51. *E. A. Bowman, D. L. Riddle, W. Kelly, Amino Acid Substitutions in the Caenorhabditis elegans RNA Polymerase II Large Subunit AMA-1/RPB-1 that Result in alpha-Amanitin Resistance and/or Reduced Function. G3 (Bethesda) **1**, 411-416 (2011).*

52. *A. L. Greenleaf, L. M. Borsett, P. F. Jiamachello, D. E. Coulter, Alpha-amanitin-resistant D. melanogaster with an altered RNA polymerase II. Cell **18**, 613-622 (1979).*

53. *S. Gronke, D. F. Clarke, S. Broughton, T. D. Andrews, L. Partridge, Molecular evolution and functional characterization of Drosophila insulin-like peptides. PLoS Genet **6**, e1000857 (2010).*

54. *O. Hahn et al., Dietary restriction protects from age-associated DNA methylation and induces epigenetic reprogramming of lipid metabolism. Genome Biol **18**, 56 (2017).*

55. *C. Selman et al., Evidence for lifespan extension and delayed age-related biomarkers in insulin receptor substrate 1 null mice. FASEB J **22**, 807-818 (2008).*

56. *S. Melnik et al., Isolation of the protein and RNA content of active sites of transcription from mammalian cells. Nat Protoc **11**, 553-565 (2016).*

57. *A. M. Bolger, M. Lohse, B. Usadel, Trimmomatic: a flexible trimmer for Illumina sequence data. Bioinformatics **30**, 2114-2120 (2014).*

58. *A. Dobin et al., STAR: ultrafast universal RNA-seq aligner. Bioinformatics **29**, 15-21 (2013).*

59. *M. I. Love, W. Huber, S. Anders, Moderated estimation of fold change and dispersion for RNA-seq data with DESeq2. Genome Biol **15**, 550 (2014).*

60. *J. R. Gerstner et al., Removal of unwanted variation reveals novel patterns of gene expression linked to sleep homeostasis in murine cortex. BMC Genomics **17**, 727 (2016).*

bioRxiv preprint doi: https://doi.org/10.1101/719864; this version posted August 8, 2019. The copyright holder for this preprint (which was not certified by peer review) is the author/funder, who has granted bioRxiv a license to display the preprint in perpetuity. It is made available under aCC-BY-NC-ND 4.0 International license.

61. *A. Liberzon et al., The Molecular Signatures Database (MSigDB) hallmark gene set collection. Cell Syst **1**, 417-425 (2015).*

62. *S. Durinck et al., BioMart and Bioconductor: a powerful link between biological databases and microarray data analysis. Bioinformatics **21**, 3439-3440 (2005).*

63. *S. Memczak et al., Circular RNAs are a large class of animal RNAs with regulatory potency. Nature **495**, 333-338 (2013).*

64. *D. Karolchik et al., The UCSC Table Browser data retrieval tool. Nucleic Acids Res **32**, D493-496 (2004).*

65. *P. Cui et al., A comparison between ribo-minus RNA-sequencing and polyA-selected RNA-sequencing. Genomics **96**, 259-265 (2010).*

66. *M. Caudron-Herger, P. R. Cook, K. Rippe, A. Papantonis, Dissecting the nascent human transcriptome by analysing the RNA content of transcription factories. Nucleic Acids Res **43**, e95 (2015).*

67. *A. Mortazavi, B. A. Williams, K. McCue, L. Schaeffer, B. Wold, Mapping and quantifying mammalian transcriptomes by RNA-Seq. Nat Methods **5**, 621-628 (2008).*

68. *J. M. Gray et al., SnapShot-Seq: a method for extracting genome-wide, in vivo mRNA dynamics from a single total RNA sample. PLoS One **9**, e89673 (2014).*

69. *X. Darzacq et al., In vivo dynamics of RNA polymerase II transcription. Nat Struct Mol Biol **14**, 796-806 (2007).*

70. *T. Hwang et al., Dynamic regulation of RNA editing in human brain development and disease. Nat Neurosci **19**, 1093-1099 (2016).*

71. *S. Diermeier et al., TNFα signalling primes chromatin for NF-κB binding and induces rapid and widespread nucleosome repositioning. Genome Biology **15**, 536 (2014).*

72. *K. Chen et al., DANPOS: dynamic analysis of nucleosome position and occupancy by sequencing. Genome Res **23**, 341-351 (2013).*

73. *M. Pertea, D. Kim, G. M. Pertea, J. T. Leek, S. L. Salzberg, Transcript-level expression analysis of RNA-seq experiments with HISAT, StringTie and Ballgown. Nat Protoc **11**, 1650-1667 (2016).*

bioRxiv preprint doi: https://doi.org/10.1101/719864; this version posted August 8, 2019. The copyright holder for this preprint (which was not certified by peer review) is the author/funder, who has granted bioRxiv a license to display the preprint in perpetuity. It is made available under aCC-BY-NC-ND 4.0 International license.

Supplementary material

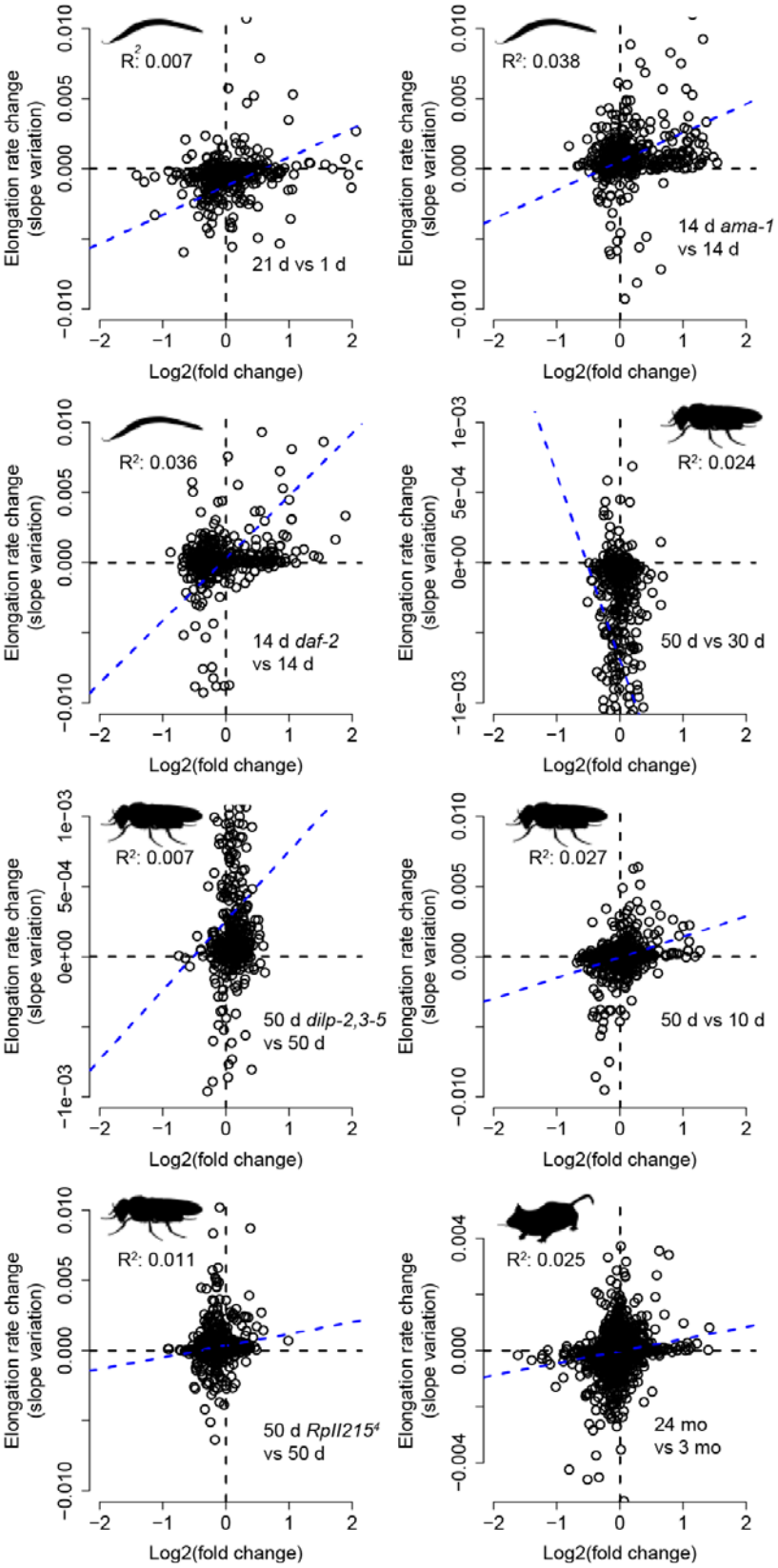

bioRxiv preprint doi: https://doi.org/10.1101/719864; this version posted August 8, 2019. The copyright holder for this preprint (which was not certified by peer review) is the author/funder, who has granted bioRxiv a license to display the preprint in perpetuity. It is made available under aCC-BY-NC-ND 4.0 International license.

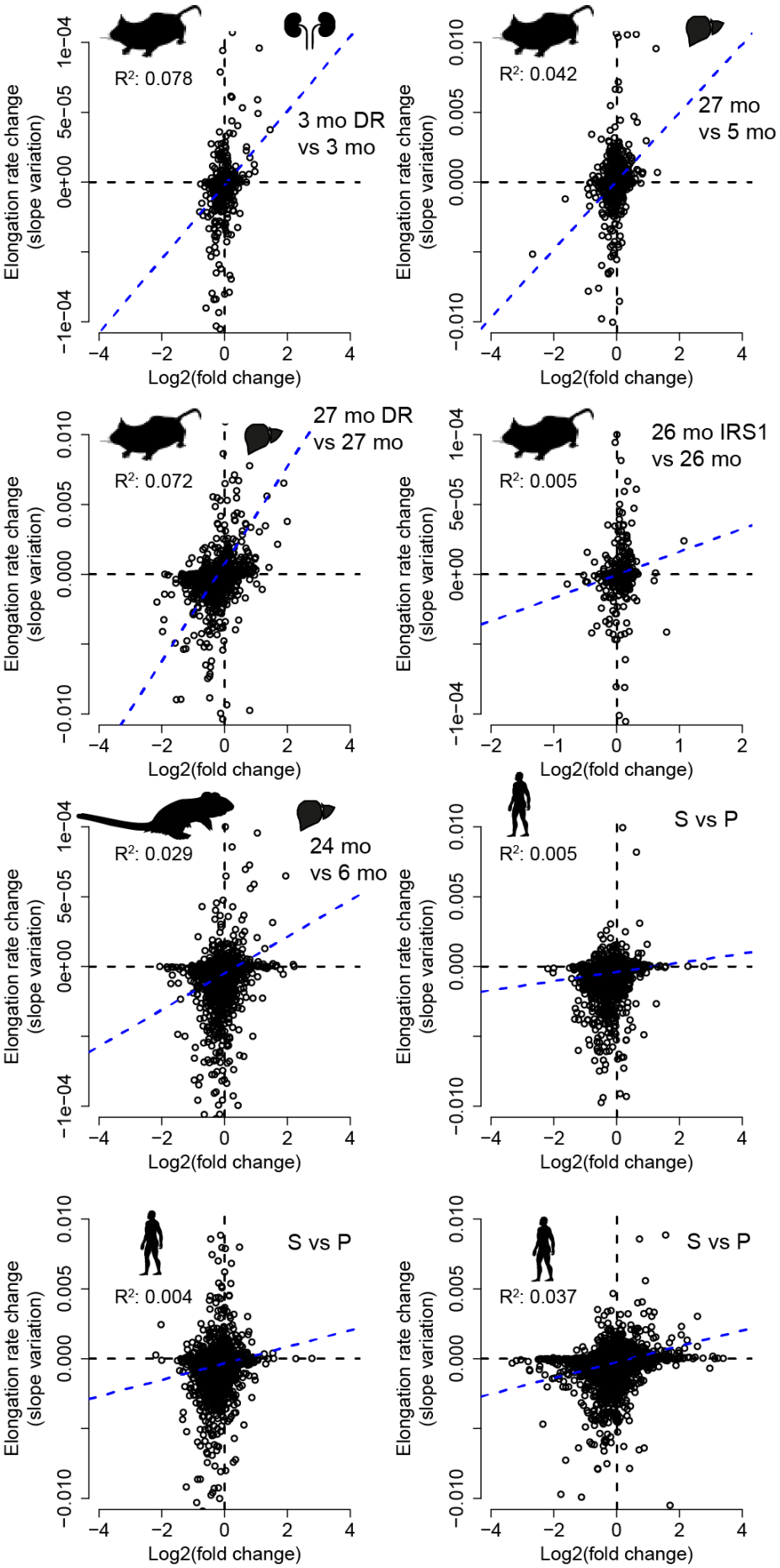

bioRxiv preprint doi: https://doi.org/10.1101/719864; this version posted August 8, 2019. The copyright holder for this preprint (which was not certified by peer review) is the author/funder, who has granted bioRxiv a license to display the preprint in perpetuity. It is made available under aCC-BY-NC-ND 4.0 International license.

Figure S1 (prev. two pages): Relationship between Pol-II speed and expression levels. Expression levels (**(**$\log_2$(fold change)) compared to Pol-II speed change for *C. elegans* (21 d vs 1 d; 14 *ama-1(m322)* d vs 14 d; 14 *daf-2* d vs 14 d), *D. melanogaster* (heads: 50 d vs 30 d; 50 *dilp2,3-5* d vs 50 d; 50 RpII215[4] d vs 50 d; 50 d vs 30 d), *M. musculus* (kidney: 24 mo vs 3 mo; 3 DR mo vs 3 mo), *R. norvegicus* (liver: 24 mo vs 6 mo), *H. sapiens* (HUVECs&IMR90: Senescent vs Proliferating). Between 0.01% and 8 % of the Pol-II speed change can be explained by mature RNA expression level variation across comparison of our studies.

bioRxiv preprint doi: https://doi.org/10.1101/719864; this version posted August 8, 2019. The copyright holder for this preprint (which was not certified by peer review) is the author/funder, who has granted bioRxiv a license to display the preprint in perpetuity. It is made available under aCC-BY-NC-ND 4.0 International license.

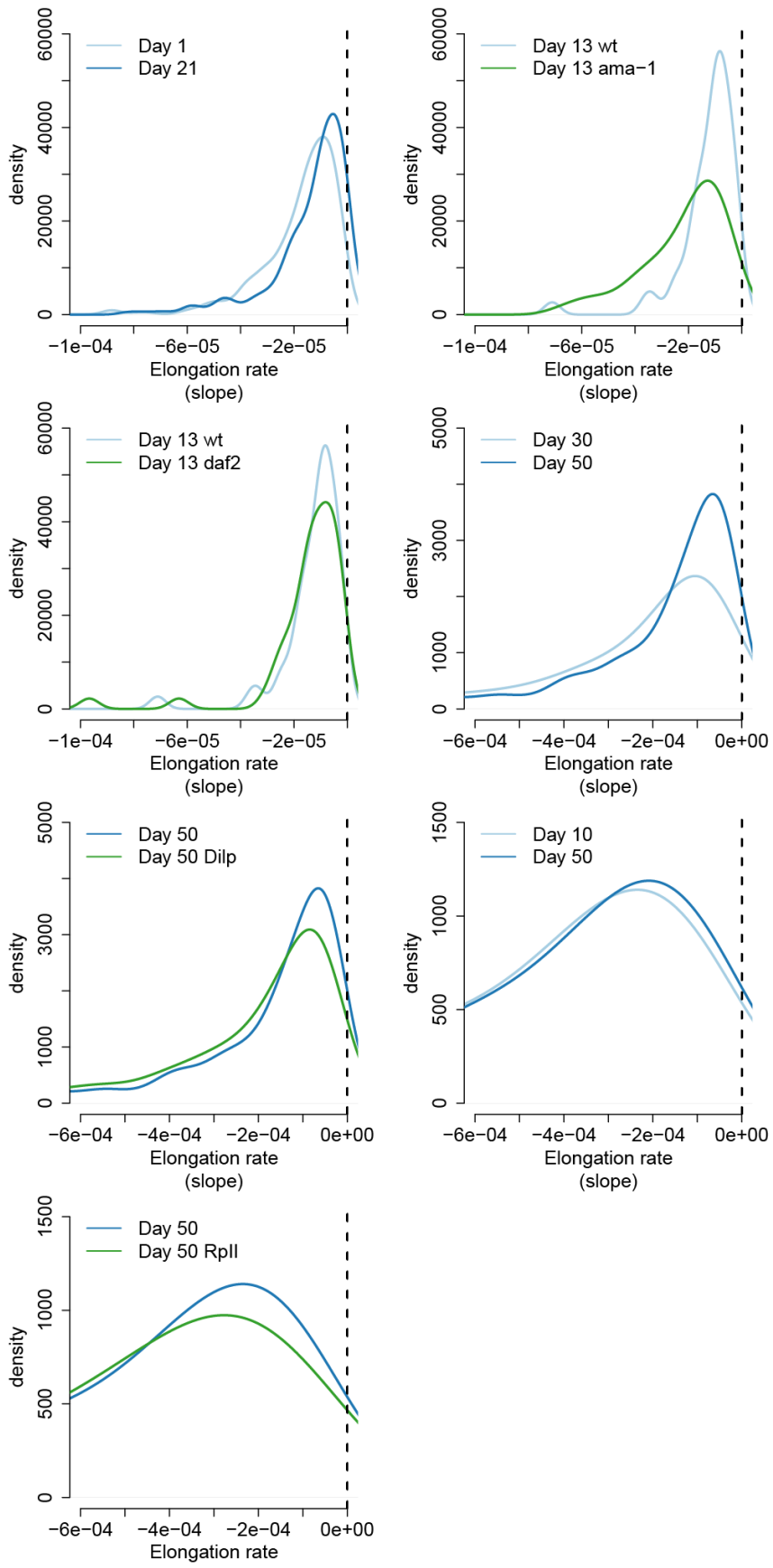

bioRxiv preprint doi: https://doi.org/10.1101/719864; this version posted August 8, 2019. The copyright holder for this preprint (which was not certified by peer review) is the author/funder, who has granted bioRxiv a license to display the preprint in perpetuity. It is made available under aCC-BY-NC-ND 4.0 International license.

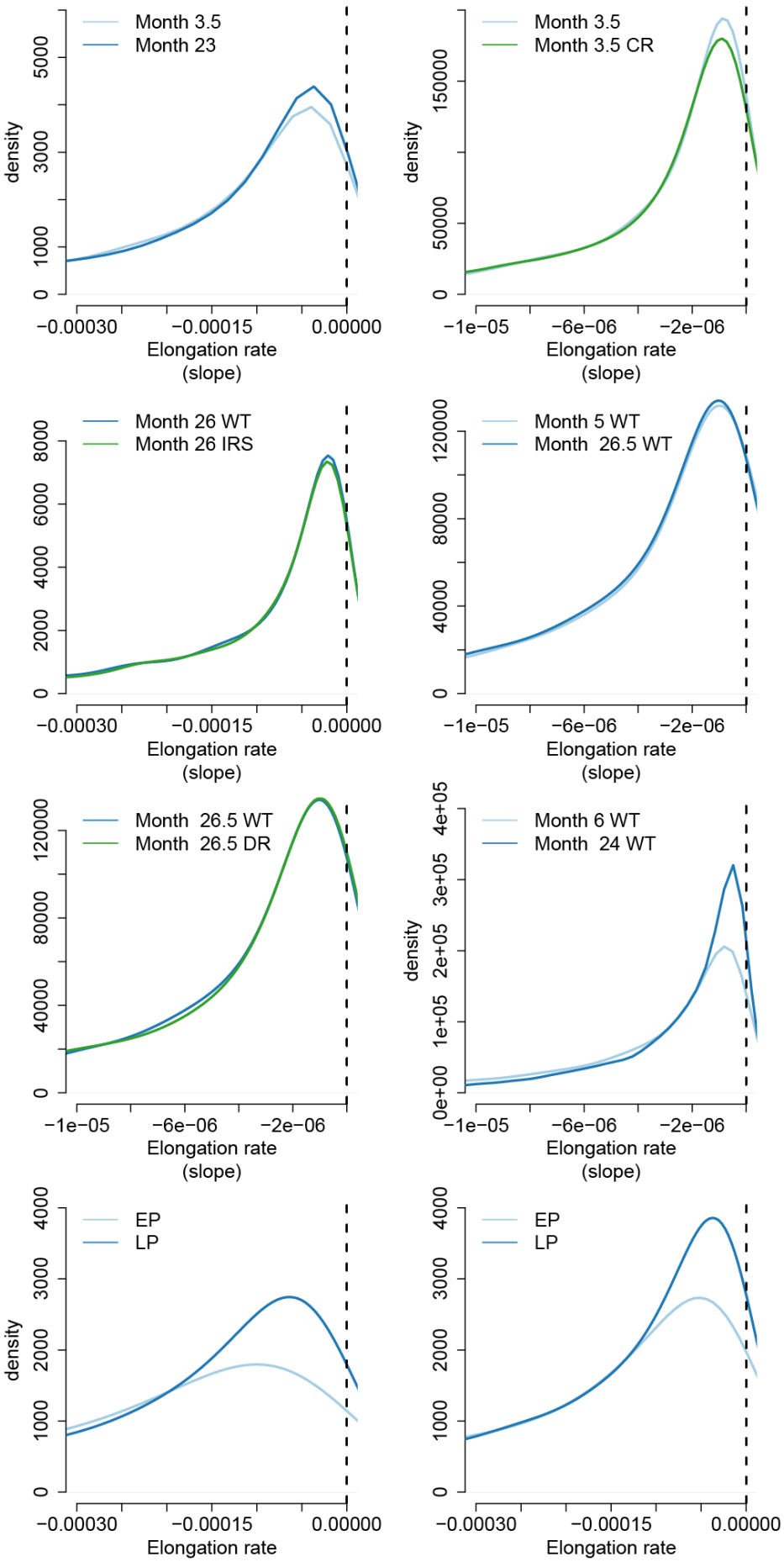

bioRxiv preprint doi: https://doi.org/10.1101/719864; this version posted August 8, 2019. The copyright holder for this preprint (which was not certified by peer review) is the author/funder, who has granted bioRxiv a license to display the preprint in perpetuity. It is made available under aCC-BY-NC-ND 4.0 International license.

Figure S2 (prev. two pages): Density distribution of intronic slope for each conditions and species (C. elegans, D. melanogaster, M. musculus, R. norvegicus, H. sapiens (EP: Early passage, LP: Late passage).

bioRxiv preprint doi: https://doi.org/10.1101/719864; this version posted August 8, 2019. The copyright holder for this preprint (which was not certified by peer review) is the author/funder, who has granted bioRxiv a license to display the preprint in perpetuity. It is made available under aCC-BY-NC-ND 4.0 International license.

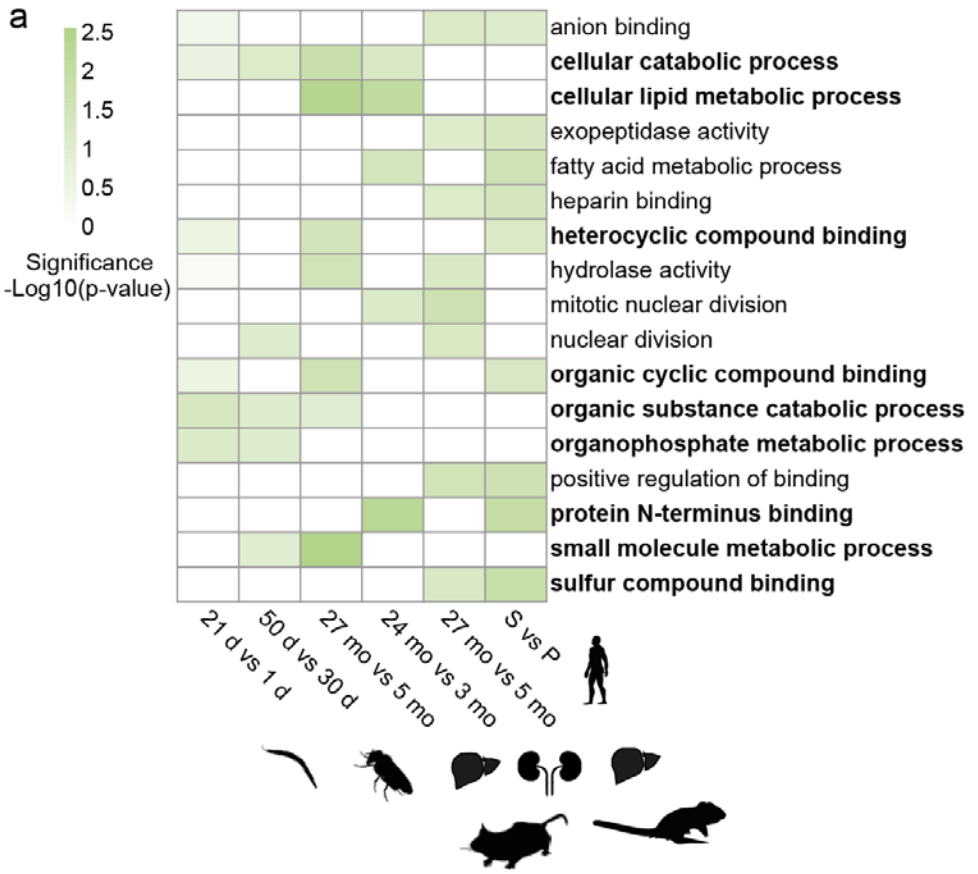

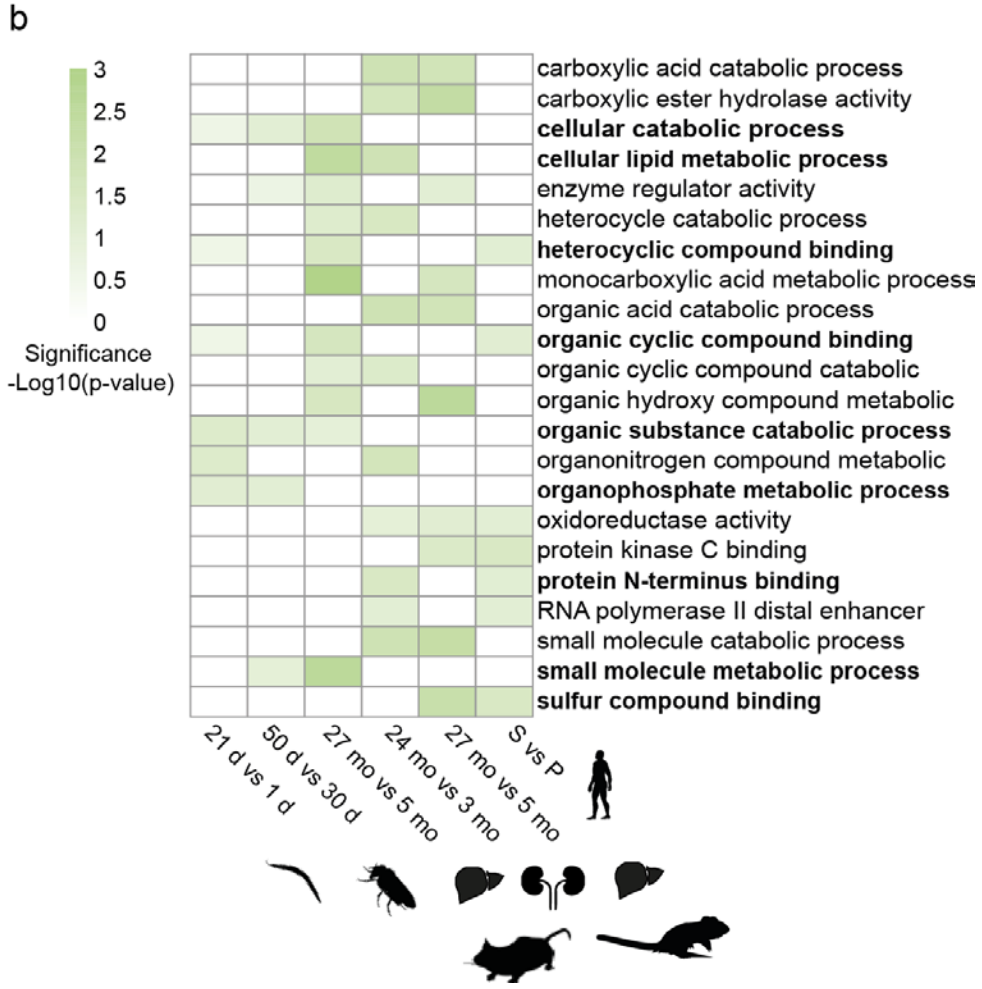

bioRxiv preprint doi: https://doi.org/10.1101/719864; this version posted August 8, 2019. The copyright holder for this preprint (which was not certified by peer review) is the author/funder, who has granted bioRxiv a license to display the preprint in perpetuity. It is made available under aCC-BY-NC-ND 4.0 International license.

Figure S3 (prev. page): Genes with increase in Pol-II speed are associated with metabolism and catabolism related pathway. GO enrichment analysis for genes harboring increasing Pol-II speed change for *C. elegans* (21 d vs 1 d), *D. melanogaster* (heads: 50 d vs 30 d), *M. musculus* (kidney: 24 mo vs 3 mo), *R. norvegicus* (liver: 24 mo vs 6 mo), *H. sapiens* (IMR90: Senescent vs Proliferating). Using as target set for GO enrichment **A,** top 200 **B,** top 300 genes with an increase in Pol-II speed change for each species (common terms between the two set top 200 and top 300 in **bold**). Color scale represent the significance of enrichment test (all GO term enriched with a p-values under 0.05, with at least more than 10 significant genes for each GO categories, Fisher elim test).

bioRxiv preprint doi: https://doi.org/10.1101/719864; this version posted August 8, 2019. The copyright holder for this preprint (which was not certified by peer review) is the author/funder, who has granted bioRxiv a license to display the preprint in perpetuity. It is made available under aCC-BY-NC-ND 4.0 International license.

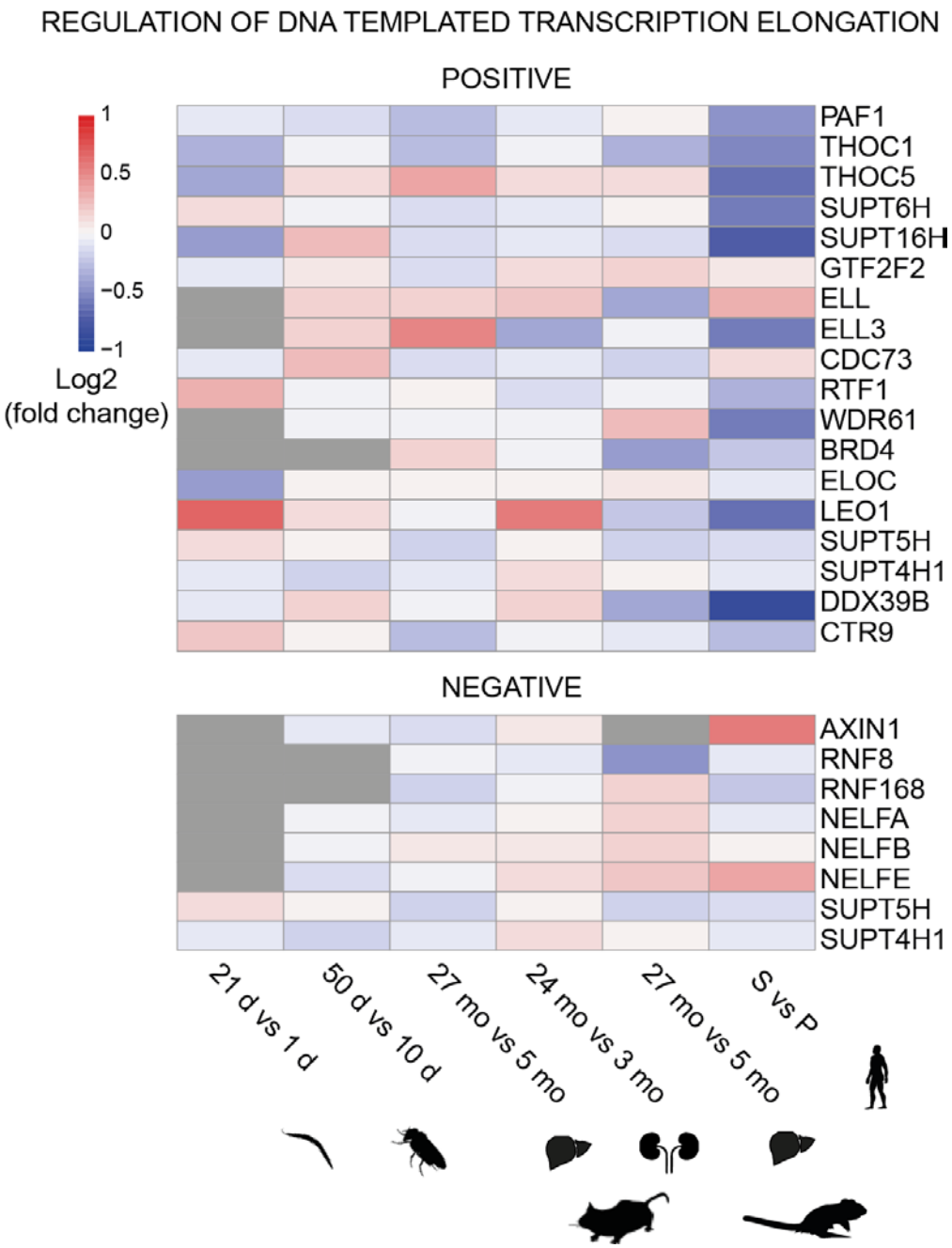

Figure S4: Heat map of differential expression (log_2 fold change) of GSEA/MSigDB (*61*) annotated genes for 'regulation of DNA templated transcriptional elongation'. Top: activators of transcriptional elongation (POSITIVE); **Bottom**: repressors of transcriptional elongation (NEGATIVE). Data shown for *WT* aging time courses: worm (21 d vs 1 d), fly heads (50 d vs 10 d), mouse liver (27 mo vs 5 mo), mouse kidneys (24 mo vs 3 mo) and human fibroblast cell line (IMR90: Senescent vs proliferating).

bioRxiv preprint doi: https://doi.org/10.1101/719864; this version posted August 8, 2019. The copyright holder for this preprint (which was not certified by peer review) is the author/funder, who has granted bioRxiv a license to display the preprint in perpetuity. It is made available under aCC-BY-NC-ND 4.0 International license.

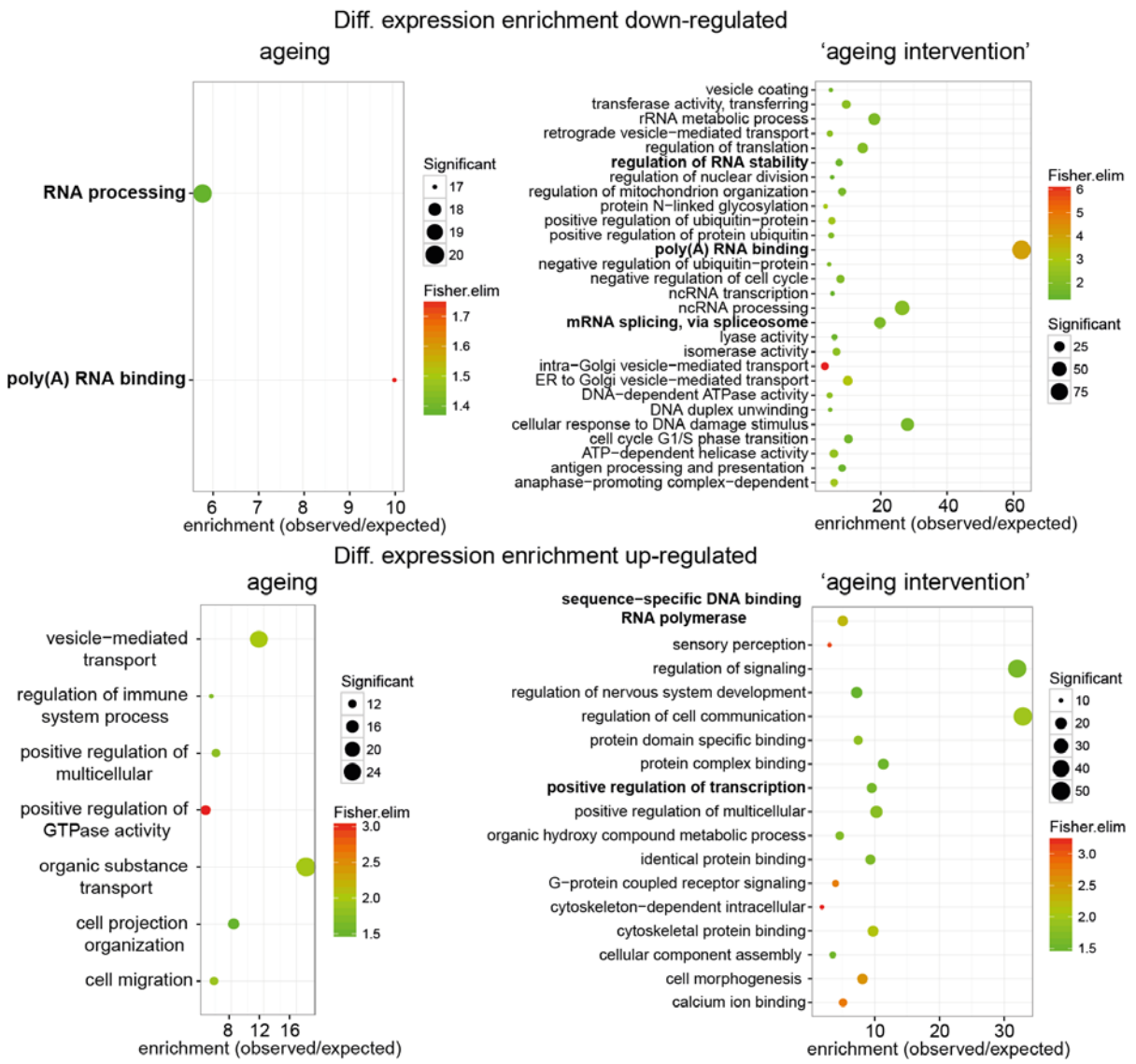

Figure S5: Functional enrichment for across-species differential expression analysis. GO enrichement for consistently up-regulated or down-regulated genes across species during aging or 'aging intervention' (as target set: aging up-regulated: 92 genes; aging down-regulated: 71; 'aging intervention' up-regulated: 164 genes; 'aging intervention' down-regulated: 473 genes; as background set 4784 orthologue genes between *H. sapiens*, *R. norvegicus*, *M. musculus*, *D. melanogaster*, *C. elegans*, all p-values *P < 0.05, significant genes > 10, fisher elim test). GO terms related to transcription and splicing in bold.

bioRxiv preprint doi: https://doi.org/10.1101/719864; this version posted August 8, 2019. The copyright holder for this preprint (which was not certified by peer review) is the author/funder, who has granted bioRxiv a license to display the preprint in perpetuity. It is made available under aCC-BY-NC-ND 4.0 International license.

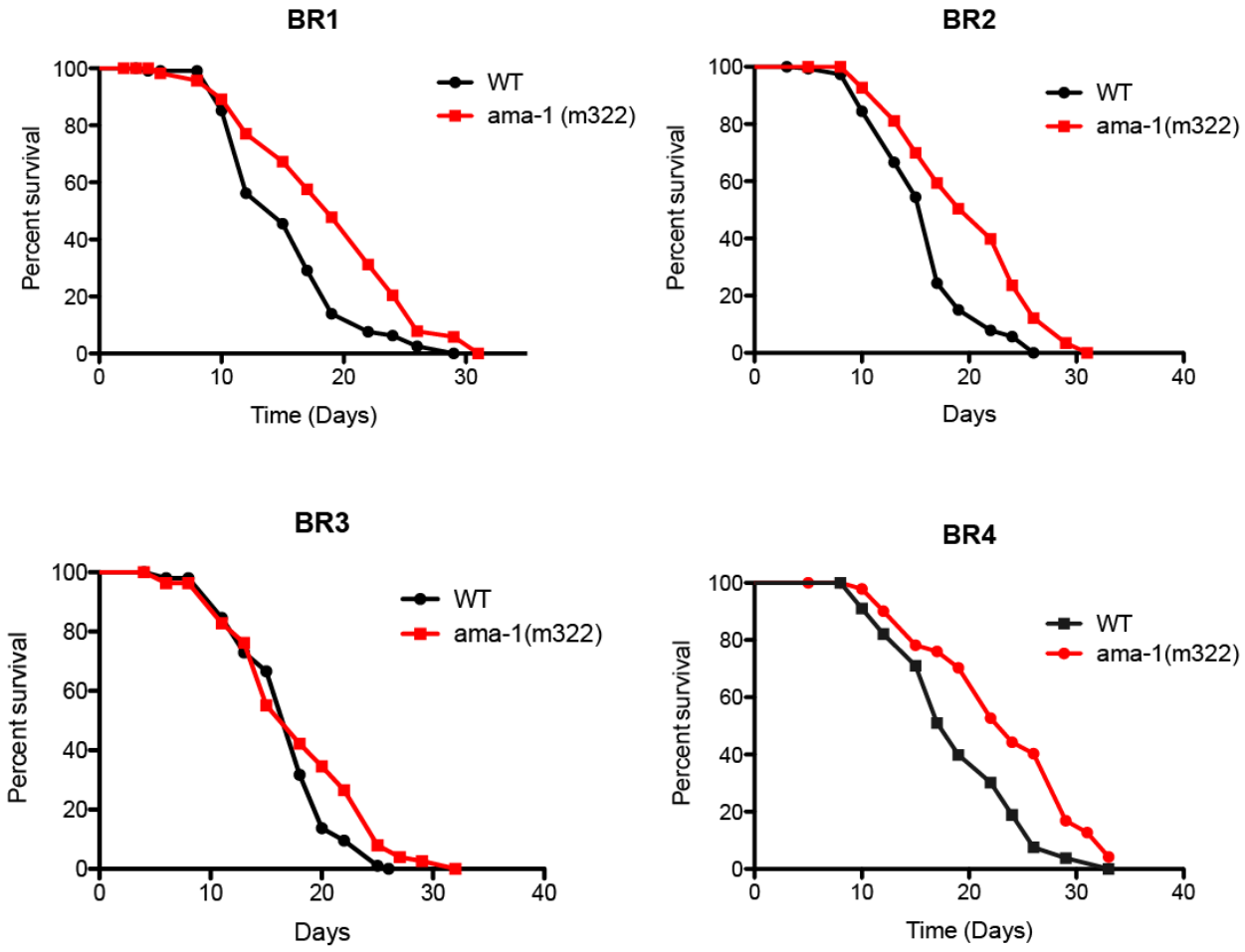

Figure S6: Slowing down Pol-II in *C. elegans* increases lifespan. Survival of wild-type and *ama-1(m322)* mutant worms conferring a slow Pol-II elongation rate (4 replicates, BR1:1.267, P < 0,0001; BR2:1.23,P < 0.0001; BR3:1, P = 0.0342; BR4:1.263,P < 0.0001, log-rank test, Mantel-cox).

bioRxiv preprint doi: https://doi.org/10.1101/719864; this version posted August 8, 2019. The copyright holder for this preprint (which was not certified by peer review) is the author/funder, who has granted bioRxiv a license to display the preprint in perpetuity. It is made available under aCC-BY-NC-ND 4.0 International license.

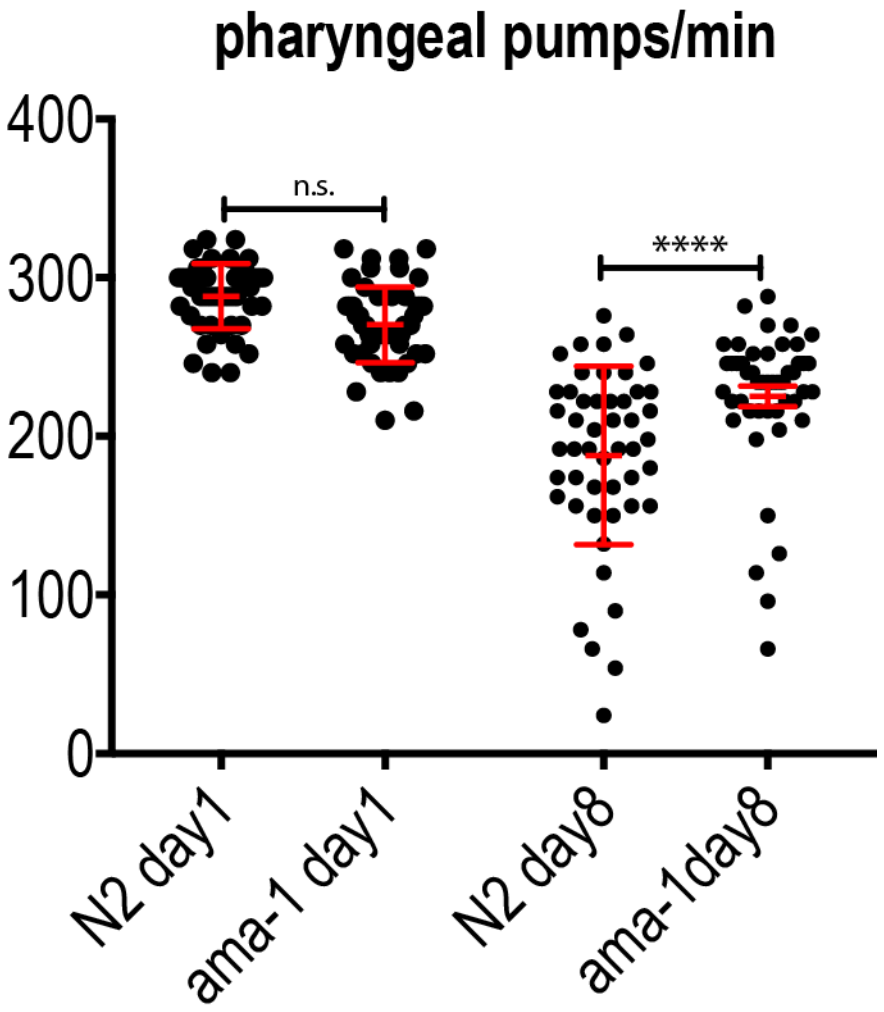

Figure S7: Slowing down Pol-II in C. elegans improves health in old age. The pumping rates of the N2 and ama-1 worms at day 1 and day 8. There is no difference on day1, but ama-1 worms overall are having much better pumping rates compared to wild types on day8, which correlates with slow aging. Wild types show on the other hand a more heterogeneous pumping rate profile.

bioRxiv preprint doi: https://doi.org/10.1101/719864; this version posted August 8, 2019. The copyright holder for this preprint (which was not certified by peer review) is the author/funder, who has granted bioRxiv a license to display the preprint in perpetuity. It is made available under aCC-BY-NC-ND 4.0 International license.

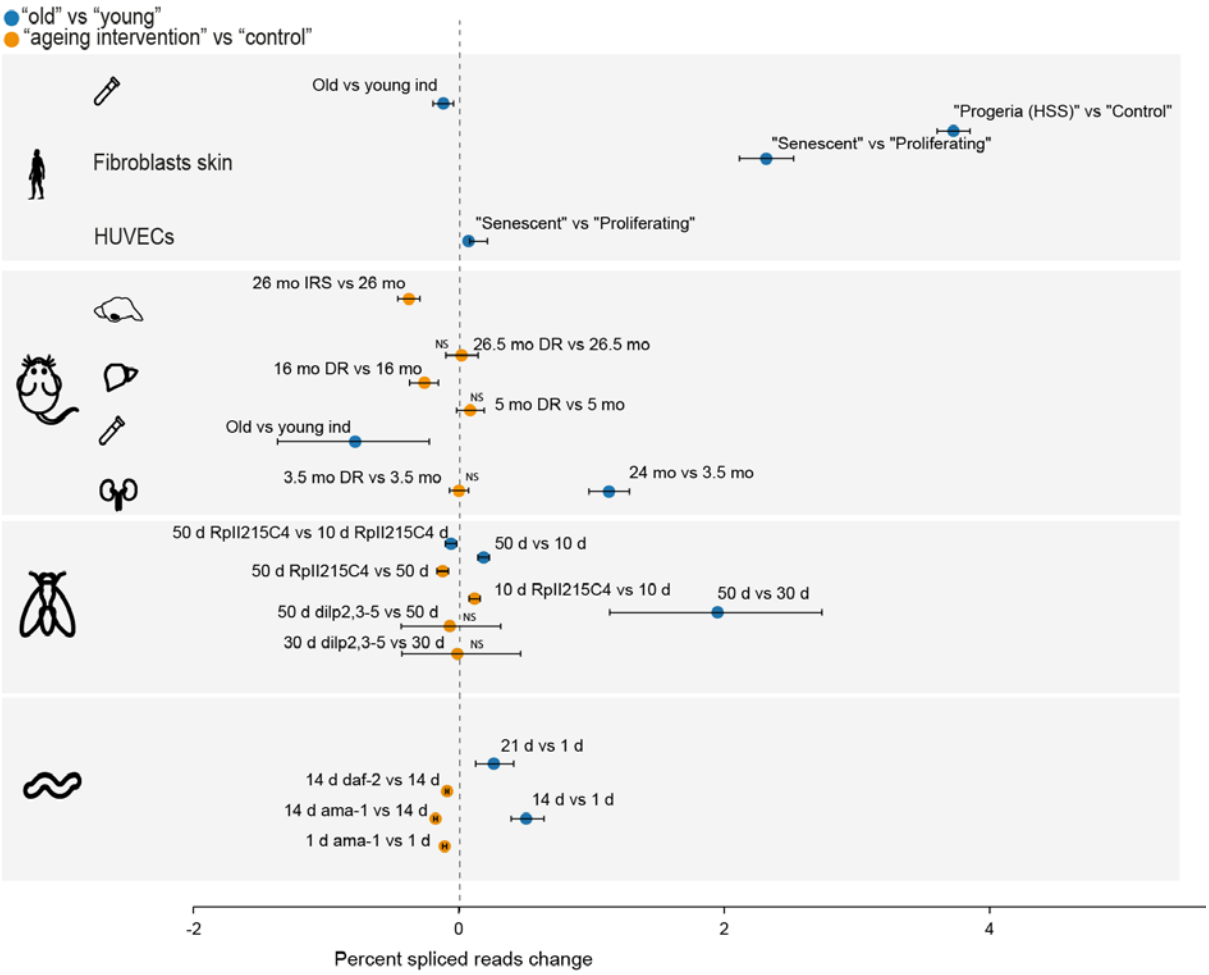

Figure S8: Percent spliced reads increases mostly with age and is often reduced upon slowdown of Pol-II. Average changes of the fraction of spliced transcripts in worm (whole body), fruit fly (brains), mouse (kidney, liver, hypothalamus), rat (liver) and human cell culture (Fibroblast skin cells derived from a HSS progeria patient compared to a healthy control; HUVECs: umbilical vein endothelial; IMR90: fetal lung). Error bars show median variation ±95% confidence interval. All average changes of fractions of spliced reads are significantly different from zero ($P < 0.001$; paired Wilcoxon rank test), except those labeled NS (not significant). Number of genes considered (n) ranged from 124 to 15328.

bioRxiv preprint doi: https://doi.org/10.1101/719864; this version posted August 8, 2019. The copyright holder for this preprint (which was not certified by peer review) is the author/funder, who has granted bioRxiv a license to display the preprint in perpetuity. It is made available under aCC-BY-NC-ND 4.0 International license.

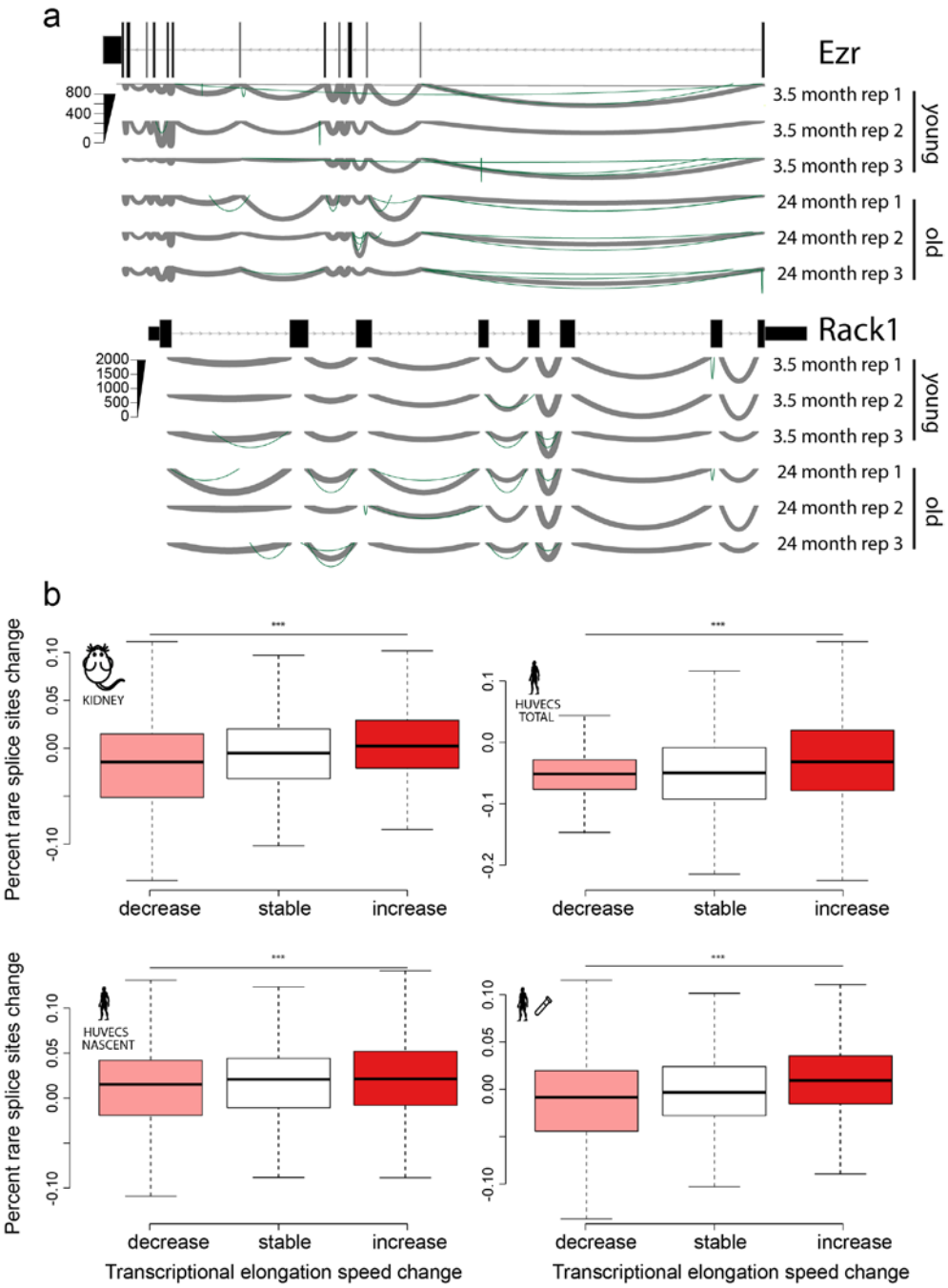

Figure S9: Examples of rare splice sites changes a) for gene Ezr and Rack1 with 3 replicates young (3.5 month) and old (26 month). Line thickness encodes the number of reads supporting this junction. Rare splice sites are shown in green. **b)** Changes in the fraction of rare splice junctions as a function of Pol-II elongation speed changes.. (Top mouse kidney, human HUVECs total, bottom: human HUVECs nascent, human blood). The differences in mean rare splice site junctions are always significantly different between genes with increased versus decreased elongation speed (***P < 0.001; paired Wilcoxon rank test).

bioRxiv preprint doi: https://doi.org/10.1101/719864; this version posted August 8, 2019. The copyright holder for this preprint (which was not certified by peer review) is the author/funder, who has granted bioRxiv a license to display the preprint in perpetuity. It is made available under aCC-BY-NC-ND 4.0 International license.

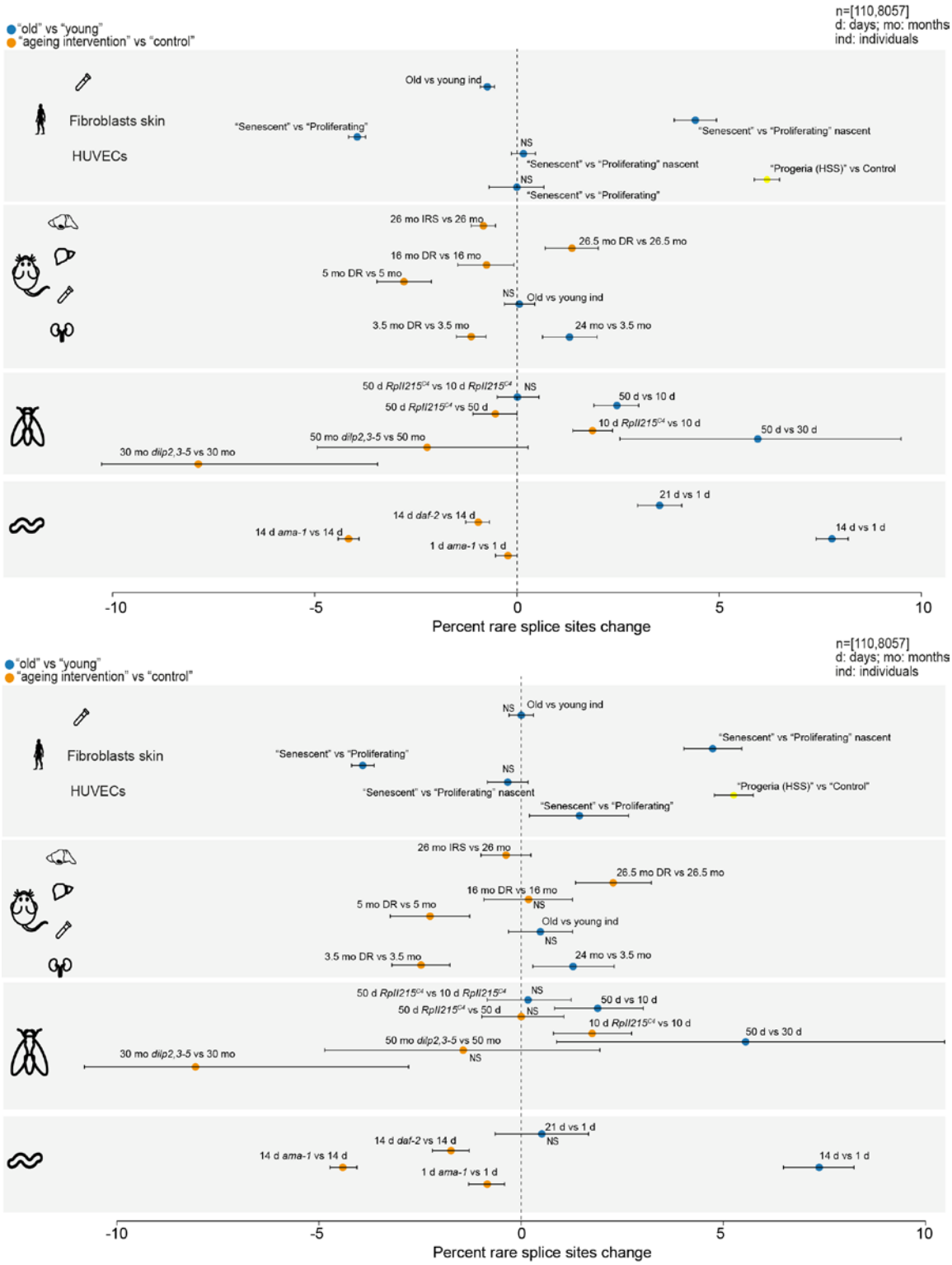

Figure S10: Percent of rare splice events change per gene. Average percent changes of rare splice events (a) <= 0.04 and b) <=0.1 percent of total gene expression) with age (blue) and upon lifespan extending treatments (orange). Error bars show median variation ±95% confidence interval. All changes of average rare splice events are significantly different from zero (P < 0.001; paired Wilcoxon rank test), except those labeled NS (not significant), **P < 0.01, *: P < 0.05. Number of genes considered (*n*) ranged from 110 to 8057.

bioRxiv preprint doi: https://doi.org/10.1101/719864; this version posted August 8, 2019. The copyright holder for this preprint (which was not certified by peer review) is the author/funder, who has granted bioRxiv a license to display the preprint in perpetuity. It is made available under aCC-BY-NC-ND 4.0 International license.

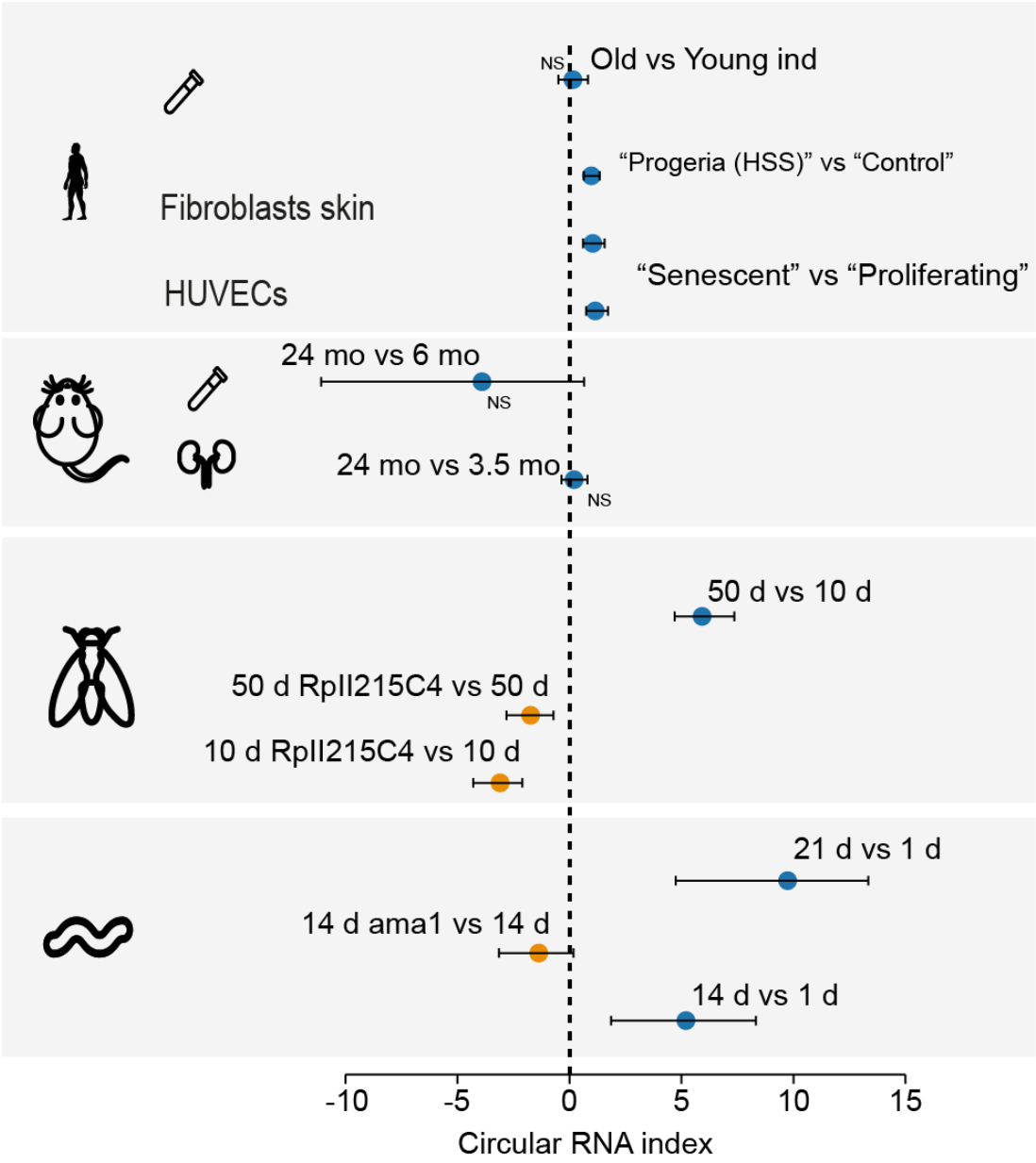

Figure S11: Formation of circular RNAs during aging and under RNA Pol-II slow mutants. Circular RNA index back-splice reads divided by linear splice reads for worms, fly heads, mouse and rat liver, human cell lines. All changes significantly different from zero at $p < 0.01$ except those labeled NS: non-significant. Blue for aging or senescence comparison. Orange for RNA Pol-II slow mutants. Yellow for progeria. Error bars show median variation ±95% confidence interval.

bioRxiv preprint doi: https://doi.org/10.1101/719864; this version posted August 8, 2019. The copyright holder for this preprint (which was not certified by peer review) is the author/funder, who has granted bioRxiv a license to display the preprint in perpetuity. It is made available under aCC-BY-NC-ND 4.0 International license.

A

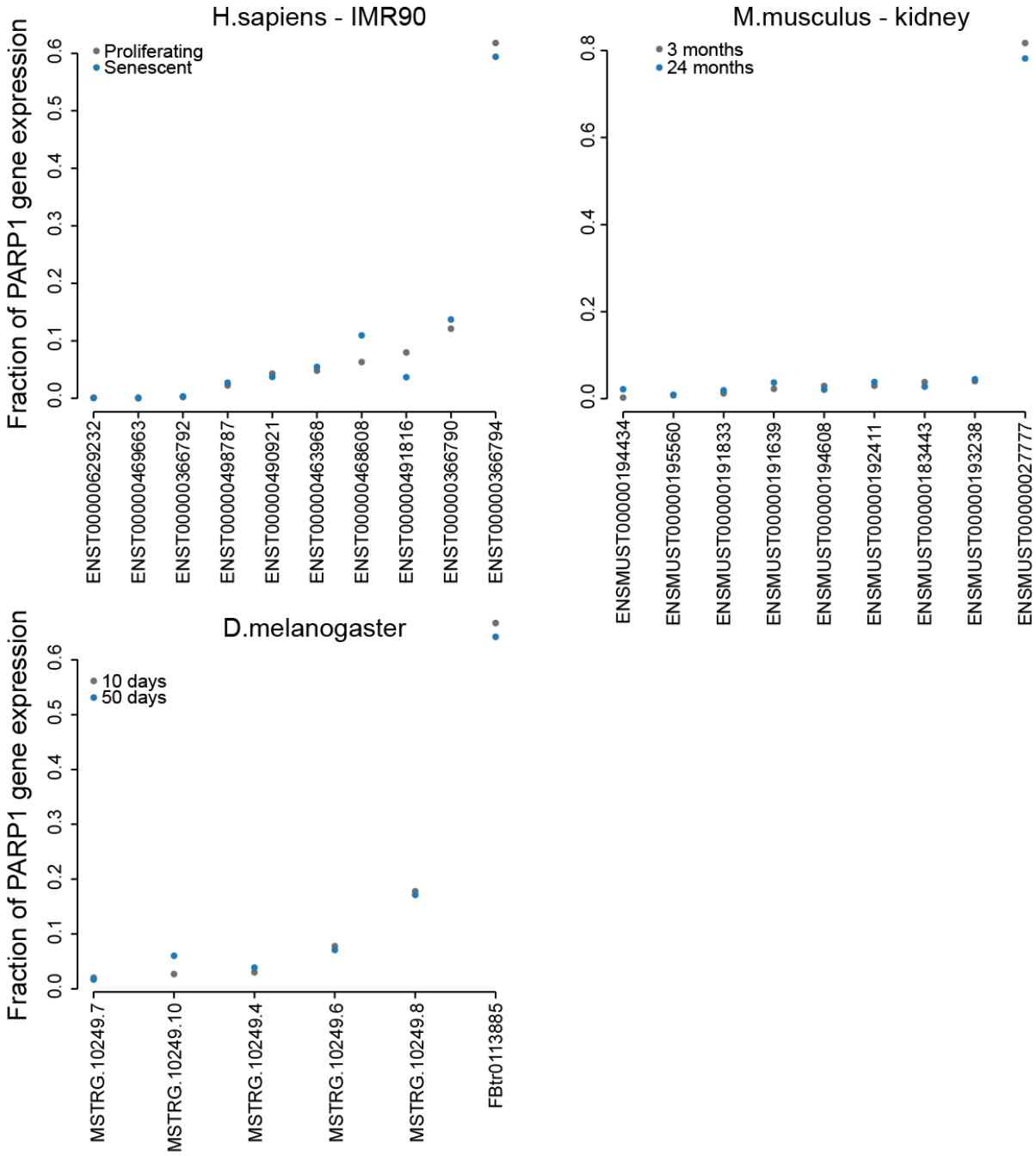

B

bioRxiv preprint doi: https://doi.org/10.1101/719864; this version posted August 8, 2019. The copyright holder for this preprint (which was not certified by peer review) is the author/funder, who has granted bioRxiv a license to display the preprint in perpetuity. It is made available under aCC-BY-NC-ND 4.0 International license.

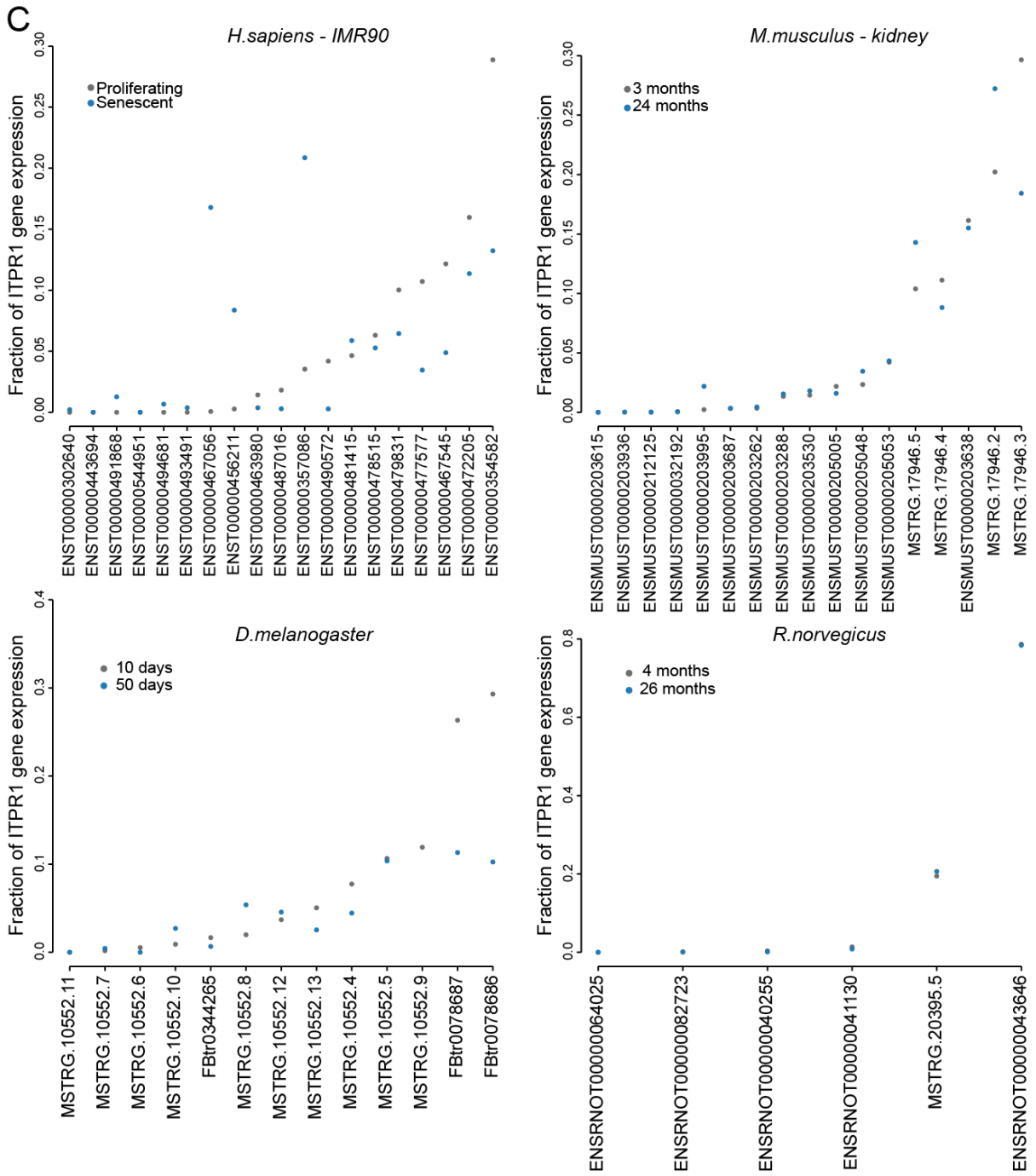

Figure S12: Decline of PARP1 and ITPR1 main isoform and increase in unannotated isoforms in fibroblast (IMR90) cell lines, mouse kidney, fly brain and rat liver. (**A**) Dotplots representing the fraction of PARP1 gene expression for each transcripts annotated by ENSEMBL or detected by StringTie (*73*). Rat data not presented as only one transcript and no new transcript could be identified by StringTie. (**B**) The alternative isoform represent only a small portion of the main isoform. **(C)** Dotplots representing the fraction of ITPR1 gene expression for each transcripts annotated by ENSEMBL or detected by StringTie (*73*). Quantification of transcript abundance was obtain using StringTie.

bioRxiv preprint doi: https://doi.org/10.1101/719864; this version posted August 8, 2019. The copyright holder for this preprint (which was not certified by peer review) is the author/funder, who has granted bioRxiv a license to display the preprint in perpetuity. It is made available under aCC-BY-NC-ND 4.0 International license.

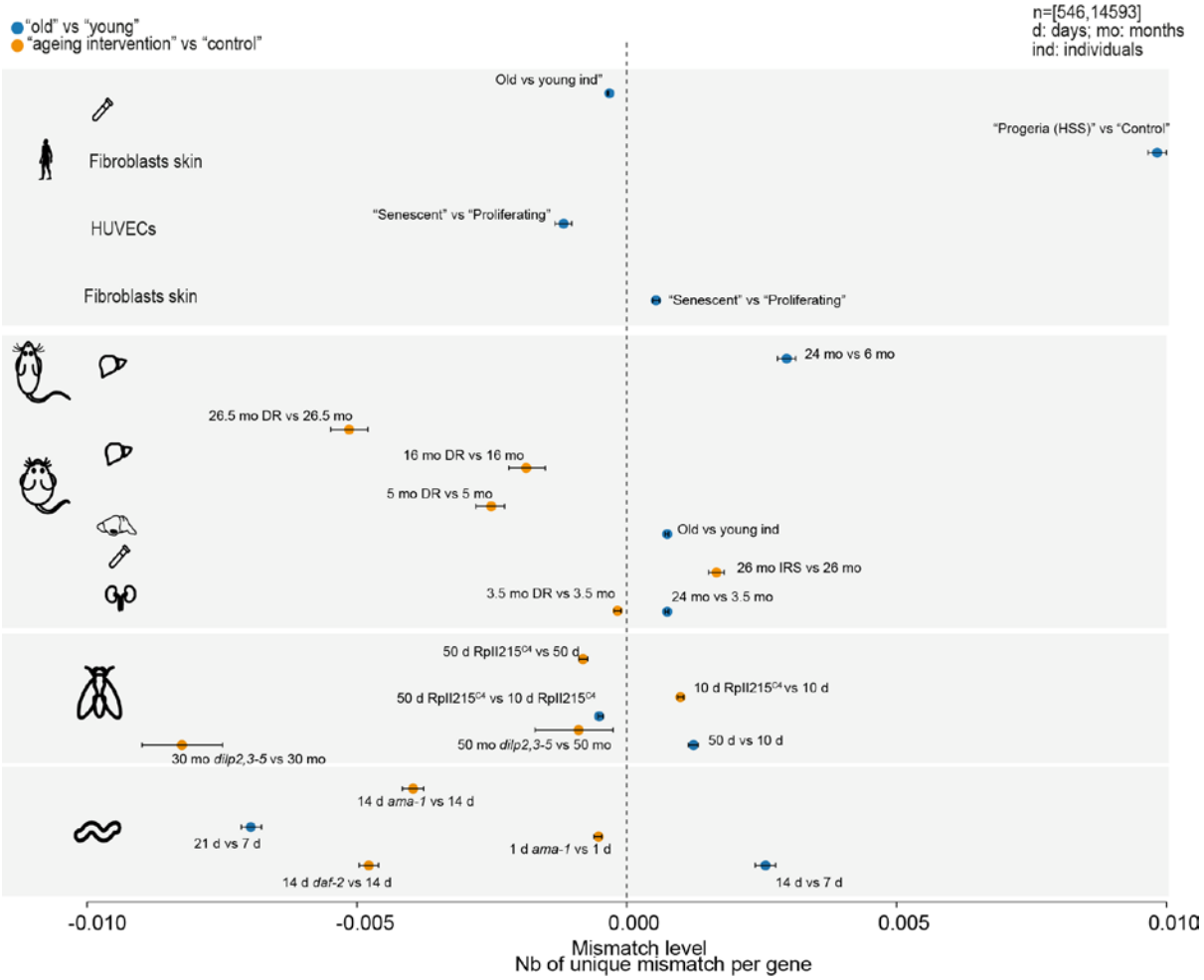

Figure S13: Mismatch level changes during aging and under lifespan-extending interventions. Average mismatch level changes with age (blue) and upon lifespan-extending treatments (orange). Error bars show median variation ±95% confidence interval. All changes of average mismatches are significantly different from zero ($P < 0.05$; paired Wilcoxon rank test). Number of genes considered (*n*) ranged from 546 to 14593.

bioRxiv preprint doi: https://doi.org/10.1101/719864; this version posted August 8, 2019. The copyright holder for this preprint (which was not certified by peer review) is the author/funder, who has granted bioRxiv a license to display the preprint in perpetuity. It is made available under aCC-BY-NC-ND 4.0 International license.

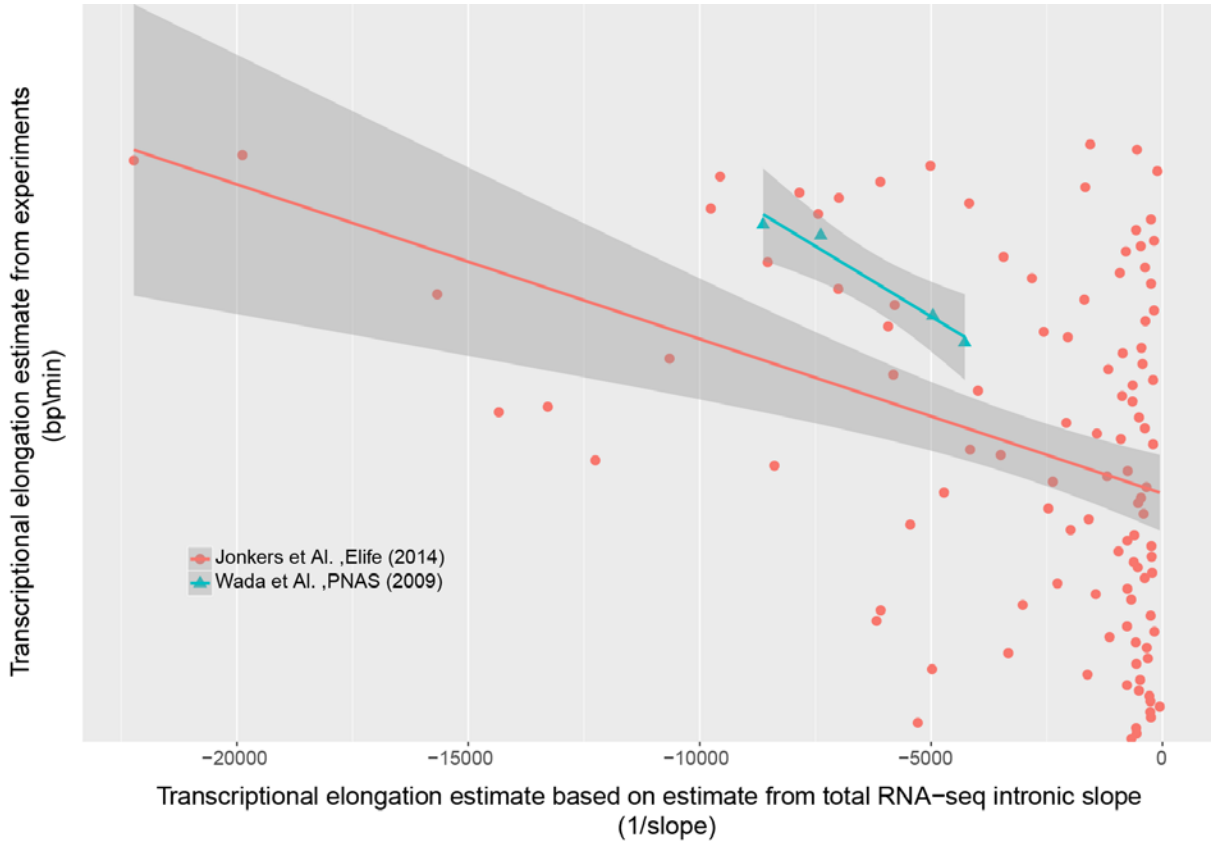

Figure S14: Correlation of transcriptional elongation estimate from GRO-seq (*15*) and tilling micro-array time series (*11*) with total RNA intronic gradient. Scatter plot of transcriptional elongation estimate from GRO-seq and tilling microarray time series versus gene-averaged transcriptional elongation estimate from total RNA-seq intron gradient. Each dot represents represent one gene (GRO-seq: Pearson correlation= 0.38, p-value= 4e-05; Tilling microarray: Pearson correlation= x, p-value= x). Red and blue line represent linear fit with 95% confidence interval for comparison with GRO-seq and tilling array respectively.

bioRxiv preprint doi: https://doi.org/10.1101/719864; this version posted August 8, 2019. The copyright holder for this preprint (which was not certified by peer review) is the author/funder, who has granted bioRxiv a license to display the preprint in perpetuity. It is made available under aCC-BY-NC-ND 4.0 International license.

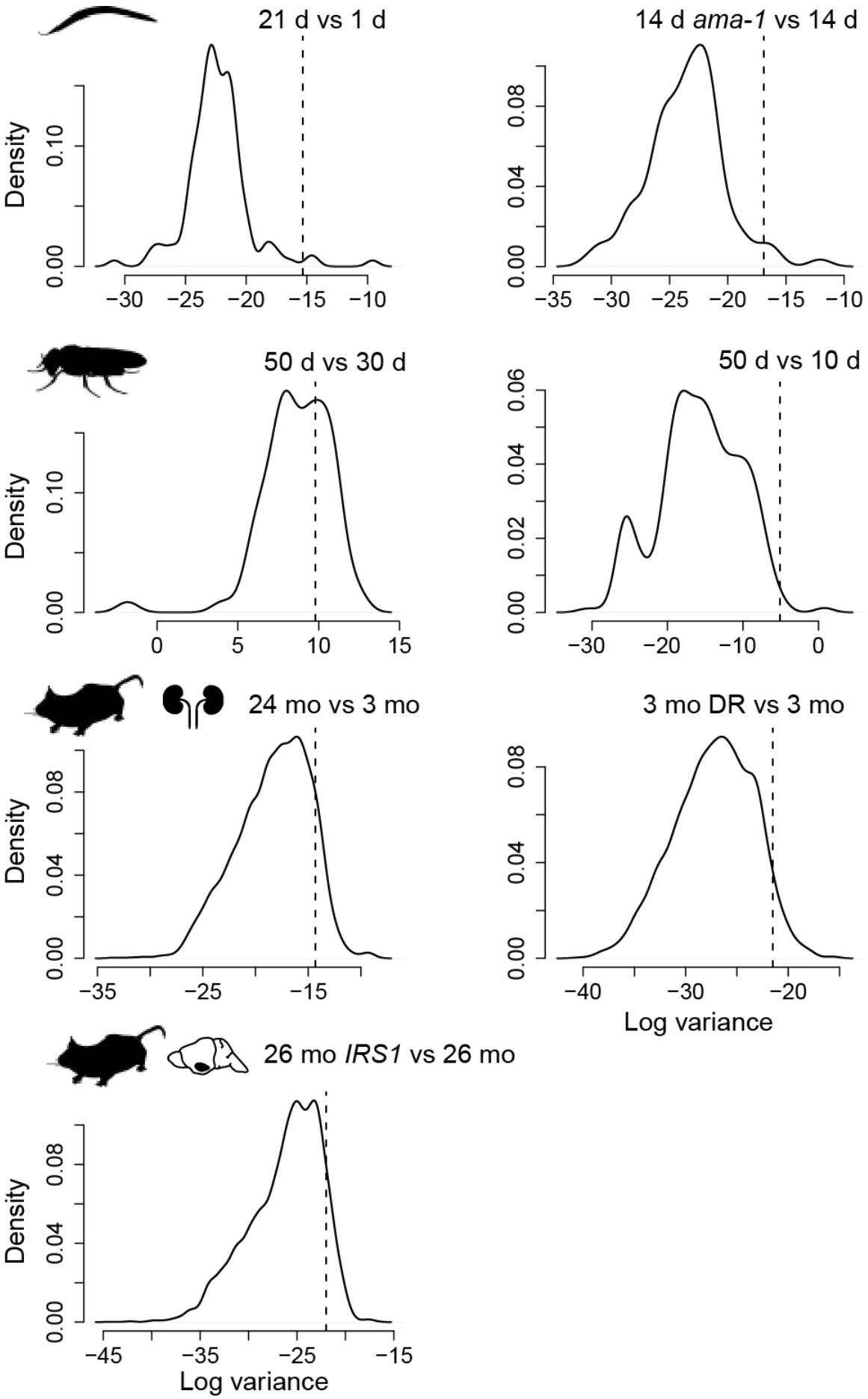

bioRxiv preprint doi: https://doi.org/10.1101/719864; this version posted August 8, 2019. The copyright holder for this preprint (which was not certified by peer review) is the author/funder, who has granted bioRxiv a license to display the preprint in perpetuity. It is made available under aCC-BY-NC-ND 4.0 International license.

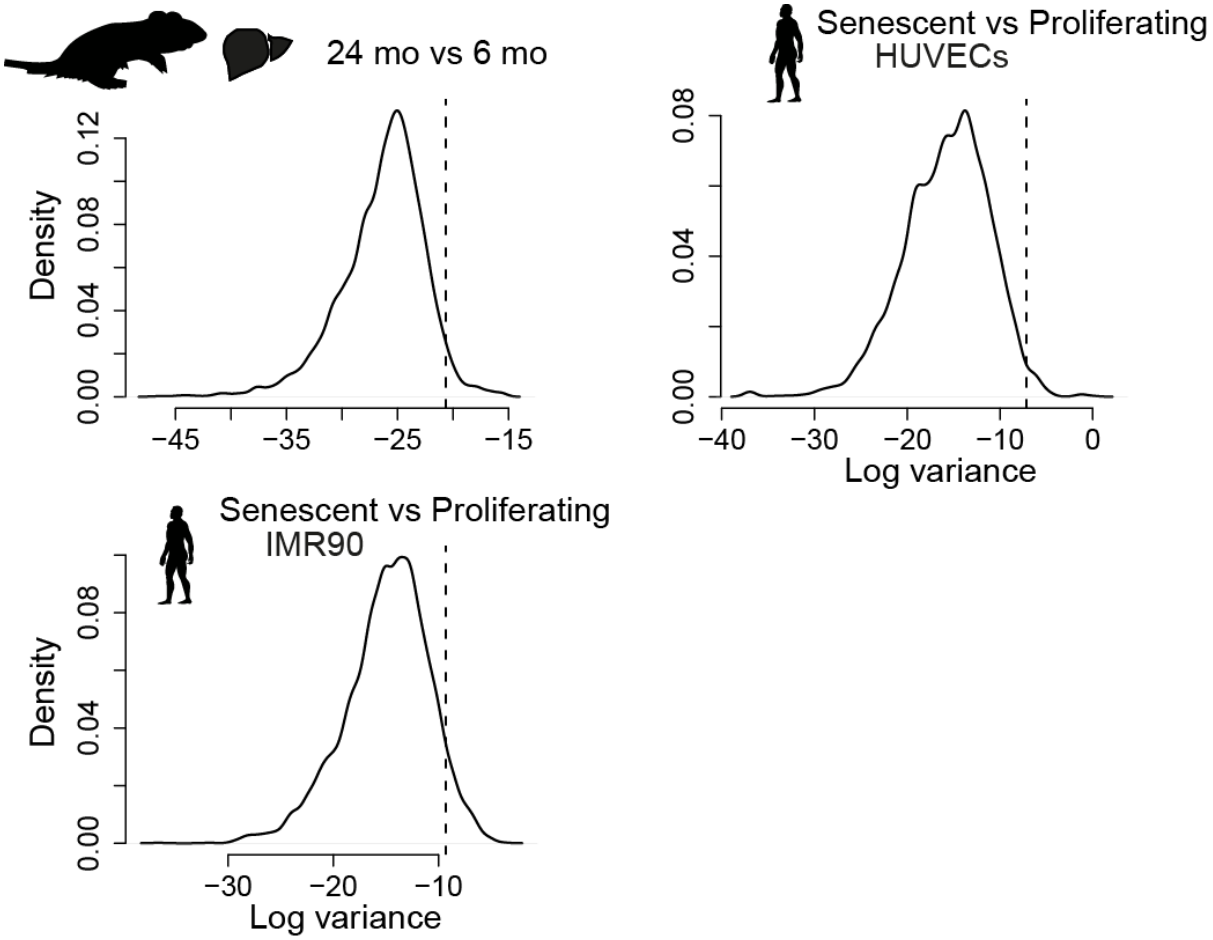

Figure S15 (prev. & this page): **Variation of Pol-II elongation speeds for different introns of the same gene.** Distribution of variances of Pol-II speed estimates (slope per intron) for introns within the same gene. Average variance of speed estimates across all introns (i.e. between genes; global average) is shown as a dashed vertical line for *C. elegans* (21 d vs 1 d; 14 *daf-2* d vs 14 d), *D. melanogaster* (heads 50 d vs 30 d; 50 d vs 10 d), *M. musculus* (kidney: 24 mo vs 3 mo; 3 DR mo vs 3 mo), *R. norvegicus* (liver: 24 mo vs 6 mo), *H. sapiens* (Umbilical vein endothelial (HUVECs); fibroblast fetal lungs (IMR90): Senescent vs Proliferating). The vast majority of intra-gene variances are below the average inter-gene variance, suggesting that introns of the same gene have coupled Pol-II elongation speeds.

bioRxiv preprint doi: https://doi.org/10.1101/719864; this version posted August 8, 2019. The copyright holder for this preprint (which was not certified by peer review) is the author/funder, who has granted bioRxiv a license to display the preprint in perpetuity. It is made available under aCC-BY-NC-ND 4.0 International license.

Species	**Tissue**	**Enrichment protocol**	**Sequencing parameters** Paired-end/single-end, read length in base pairs (*bp*), millions of reads (M)	**Time points[1] and conditions**
C. elegans	Whole body	TruSeq Stranded Total RNA Library	Paired-end, 75 *bp*, 25 M	Day 1 (*WT*), day 7 (*WT*), day 14 (*WT*), day 21 (*WT*)
	Whole body	TruSeq Stranded Total RNA Library	Paired-end, 75 *bp*, 25 M	Day 14 (*WT*, *daf-2(e1370)*, *ama-1(m322)*)
	Whole body	TruSeq Stranded Total RNA library	Paired-end, 75 bp, 25 M	Day 1 (WT, ama-1 (m322))
D. melanogaster	Head	TruSeq Stranded Total RNA Library	Single-end, 100 *bp*, 37.5 M	Day 30 (*WT*, *dilp2,3-5*), Day 50 (*WT*, *dilp2,3-5*)
	Head	TruSeq Stranded Total RNA Library	Paired-end, 75 *bp*, 30 M	Day 10 (*WT*, *RpII215*^{C4}), day 50 (*WT*, *RpII215*^{C4})
M. musculus	Kidney	TruSeq Stranded Total RNA Library	Paired-end, 75 *bp*, 70 M	Month 3 (*WT*), month 24 (*WT*)
	Kidney	TruSeq Stranded Total RNA Library	Paired-end, 75 *bp*, 30 M	Month 3 (*WT*, *DR*) (4 replicates)
	Liver	TruSeq Stranded Total RNA Library	Paired-end, 75 *bp*, 37.5 M	Month 5 (*WT*, *DR*)
	Liver	TruSeq Stranded Total RNA Library	Paired-end, 75 *bp*, 37.5 M	Month 16 (*WT*, *DR*)
	Liver	TruSeq Stranded Total RNA Library	Paired-end, 75 *bp*, 37.5 M	Month 27 (*WT*, *DR*)
	Blood	TruSeq Stranded Total RNA Library	Paired-end, 75 *bp*, 70 M	Month 5 *(WT)*, month 27 *(WT)*
	Hypothala-mus	TruSeq Stranded Total RNA Library	Single-end, 100 *bp*, 30 M	Month 26 (*WT*, *IRS1-/-*)
R. norvegicus (*17*)	Liver	TruSeq Stranded Total RNA Library	Single-end, 50 *bp*, 60 M	Month 6 (*WT*), month 24 (*WT*) (2 replicates)
	Brain[2]	TruSeq Stranded Total RNA Library	Single-end, 50 *bp*, 20 M	Month 6 (*WT*), month 24 (*WT*) (6 replicates)

Table S1: Description of the RNA-seq dataset used in the study. (Contd. next page.)

[1] Triplicate except mentioned otherwise.
[2] Not included in the analysis due to low coverage (bellow 1X genome coverage or 29 M sequenced reads for *R. norvegicus* ; genome coverage calculated using Lander-Waterman formula)

bioRxiv preprint doi: https://doi.org/10.1101/719864; this version posted August 8, 2019. The copyright holder for this preprint (which was not certified by peer review) is the author/funder, who has granted bioRxiv a license to display the preprint in perpetuity. It is made available under aCC-BY-NC-ND 4.0 International license.

Species	**Tissue**	**Enrichment protocol**	**Sequencing parameters** Paired-end/single-end, read length in base pairs (*bp*), millions of reads (M)	**Time points[3] and conditions**
H. sapiens	Fetal lungs (IMR90)	Nascent RNA	Paired-end, 75 *bp*, 25 M	Early passage, late passage (2 replicates)
	Fetal lungs (IMR90)	TruSeq Stranded Total RNA Library	Paired-end, 75 *bp*, 50 M	Early passage, late passage (2 replicates)
	Umbilical vein endothelial (HUVECs)	Nascent RNA	Paired-end, 75 *bp*, 50 M	Early passage, late passage (2 replicates)
	Umbilical vein endothelial (HUVECs)	TruSeq Stranded Total RNA Library	Paired-end, 75 *bp*, 100 M	Early passage, late passage
	Skin fibroblasts	TruSeq Stranded Total RNA Library	Paired-end, 100 *bp*, 100 M	Progeria patient (HSS) (2 replicates)
			Paired-end, 75 *bp*, 100 M	Healthy donor, sex/age matched with progeria patient (2 replicates)
	Blood	TruSeq Stranded Total RNA Library	Paired-end, 75 *bp*, 70 M	Healthy donor, 6 females, 6 males, age range: 21-70

Table S1: Description of the RNA-seq dataset used in the study. (Contd. from previous page.)

[3] Triplicate except mentioned otherwise.